THE FABRICATION OF VOPcPhO NANOFLOWERS AND P3HT:VOPcPhO COMPOSITE NANORODS VIA TEMPLATE-ASSISTED METHOD

ANAS KAMARUNDZAMAN

DEPARTMENT OF PHYSICS
FACULTY OF SCIENCE
UNIVERSITI MALAYA
KUALA LUMPUR

2014

UNIVERSITI MALAYA

ORIGINAL LITERARY WORK DECLARATION

Name of Candidate: Anas Bin Kamarundzaman (I.C/Passport No: 880120145385)

Registration/Matric No: SGB120002

Name of Degree: MSc Coursework Applied Physics

Title of Project Paper/Research Report/Dissertation/Thesis ("this Work"):
The Fabrication of VOPcPhO Nanoflowers and P3HT:VOPcPhO Composite Nanorods via Template-Assisted Method

Field of Study: Nanotechnology and Nanomaterials

I do solemnly and sincerely declare that:

(1) I am the sole author/writer of this Work;
(2) This Work is original;
(3) Any use of any work in which copyright exists was done by way of fair dealing and for permitted purposes and any excerpt or extract from, or reference to or reproduction of any copyright work has been disclosed expressly and sufficiently and the title of the Work and its authorship have been acknowledged in this Work;
(4) I do not have any actual knowledge nor do I ought reasonably to know that the making of this work constitutes an infringement of any copyright work;
(5) I hereby assign all and every rights in the copyright to this Work to the University of Malaya ("UM"), who henceforth shall be owner of the copyright in this Work and that any reproduction or use in any form or by any means whatsoever is prohibited without the written consent of UM having been first had and obtained;
(6) I am fully aware that if in the course of making this Work I have infringed any copyright whether intentionally or otherwise, I may be subject to legal action or any other action as may be determined by UM.

Candidate's Signature Date

Subscribed and solemnly declared before,

Witness's Signature Date

Name:
Designation:

ABSTRACT

In this study, the fabrication of vanadyl 2,9,16,23-tetraphenoxy-29H,31H phthalocyanine (VOPcPhO) nanoflowers and poly(3-hexylthiophene-2,5-diyl) (P3HT) : vanadyl 2,9,16,23-tetraphenoxy-29H,31H phthalocyanine (VOPcPhO) composite nanorods is reported. VOPcPhO nanoflowers and P3HT:VOPcPhO composite nanorods have been synthesised via the template-assisted method. VOPcPhO nanoflowers are prepared by varying the solution concentration (5 & 15mg/ml), spin coating rate (1000 & 2000 rpm) and annealing temperature (50 & 150 °C). P3HT:VOPcPhO composite nanorods have been synthesised from solution concentration of 5 mg/ml. Both VOPcPho nanoflowers and P3HT:VOPcPhO composite nanorods underwent a template's dissolution. FESEM (Field Emission Scanning Electron Microscopy) and TEM (Transmission Electron Microscopy) images explained the growth mechanism of VOPcPhO nanoflowers and P3HT:VOPcPhO composite nanorods. Their morphological and structural properties are further characterized via FESEM and TEM. UV–vis spectra of VOPcPhO nanoflowers show a wider absorption at Q-band as compared to VOPcPhO thin films. P3HT:VOPcPhO composite nanorods show a same result as VOPcPhO nanoflowers. The wider band absorption and the shifted of peak absorption to the longer wavelength is observed in UV-vis spectrum which is caused by the improved interaction between small molecules and P3HT segment at their interfaces. The changes in Raman shift have also been observed which indicate the improvement of nanostructures exhibited by VOPcPhO and P3HT:VOPcPhO composite.

ABSTRAK

Dalam kajian ini, fabrikasi bunga nano vanadyl 2,9,16,23-tetraphenoxy-29H,31H phthalocyanine (VOPcPhO) dan komposit rod nano poly(3-hexylthiophene-2,5-diyl) (P3HT) : vanadyl 2,9,16,23-tetraphenoxy-29H,31H phthalocyanine (VOPcPhO) dilaporkan. Bunga nano VOPcPhO dan komposit rod nano telah dihasilkan menggunakan kaedah bantuan acuan. Bunga nano VOPcPhO disediakan dengan memanipulasikan kepekatan larutan (5 & 15 mg/ml), kadar putaran salutan (1000 & 2000 rpm) dan suhu sepuhlindap (50 & 150 °C). Komposit rod nano P3HT:VOPcPhO telah dihasilkan daripada larutan berkepekatan 5 mg/ml. Kedua-dua bunga nanoVOPcPhO dan komposit rod nano P3HT: VOPcPhO menjalani proses penyingkiran acuan. Imej FESEM (Mikroskopi Elektron Daya Imbasan) dan TEM (Mikroskopi Elektron Transmisi) menjelaskan mekanisma pembentukan bunga nano VOPcPhO dan komposit rod nano P3HT: VOPcPhO. Morfologi dan ciri-ciri strukturnya dikaji dengan lebih terperinci menggunakan FESEM dan TEM. Spektra UV-vis bunga nano VOPcPhO menunjukan penyerapan lebih meluas di jalur-Q berbanding filem nipis VOPcPhO. Komposit rod nano P3HT:VOPcPhO menunjukan hasil yang sama seperti bunga nano VOPcPhO. Penyerapan yang meluas dan anjakan puncak penyerapan kepada panjang gelombang diperhatikan pada spektra UV-vis yang disebabkan oleh peningkatan interaksi antara molekul-molekul kecil dan segmen P3HT pada permukaanya. Perubahan pada anjakan Raman juga dapat dilihat yang menyatakan peningkatan pada struktur nano dipamerkan oleh VOPcPhO dan komposit P3HT:VOPcPhO.

ACKNOWLEDGEMENTS

It is a pleasure to thank the many people who made this thesis possible.

It is difficult to overstate my gratitude to my supervisor, Dr. Azzuliani Supangat. With her enthusiasm, her inspiration, leadership and her great efforts have set an example I hope to match someday. Throughout my thesis-writing period, she provided encouragement, sound advice and lots of good ideas. I would have been lost without her.

Thanks to Dr Khaulah Sulaiman, my co-supervisor, for making this research possible.

I'd like to thank the many staff, graduate and undergraduate students I have worked with in Low Dimensional Materials Research Center, Department of Physics in Universiti Malaya who have given me a lot of guidance and relevant knowledge: Muhamad Saipul Fakir, Muhammad Musoddiq, Mohd Arif, Fatin Farhana and Adreen Azman. The experience with all the Low Dimensional Materials Research Center staff and student has been an interesting and rewarding one.

Last but not least, I would like to thank my parents for their unconditional support, both financially and emotionally throughout my studies. In particular, the patience and understanding shown by my mum, dad during the year is greatly appreciated. Thanks Hajah Nor Hayati and Haji Kamarundzaman.

APPENDIX: PUBLICATIONS ARISING FROM THIS DISSERTATION

Part of the work presented in this dissertation has been published to refereed journals (Q1). The following is lists of publications (ISI-cited) that have arisen as a result of work presented in this thesis.

1. Anas Kamarundzaman, Muhamad Saipul Fakir, Azzuliani Supangat, Khaulah Sulaiman and Hadi Zulfiqar. "Morphological and optical properties of hierarchical tubular VOPcPhO nanoflowers", *Materials Letters*, Vol 111, 2013. pp. 13-16

2. Azzuliani Supangat, Anas Kamarundzaman, Nor Asmaliza Bakar, Khaulah Sulaiman and Hadi Zulfiqar. "P3HT:VOPcPhO composite nanorods arrays fabricated via template-assisted method: Enhancement on the structural and optical properties", *Materials Letters*, Vol 118, 2014. pp. 103-106

TABLE OF CONTENTS

LIST OF FIGURES

LIST OF TABLES

LIST OF SYMBOLS

ν	Frequency
h	Constant factor
E	Energy
π	Pi
σ	Sigma
δ	Dislocation Density

LIST OF ABBREVIATIONS

CCD	Charged coupled device
CMC	Critical micelle concentration
EDX	Energy-dispersive X-ray
Fe	Iron
FESEM	Field emission scanning electron microscope
HOMO	Highest occupied molecular orbital
LUMO	Lowest unoccupied molecular orbital
MS	Magnetic saturation
NaOH	Sodium hydroxide
P3HT	Poly(3-hexylthiophene-2,5-diyl)
PT	Phthalocyanine
rpm	Rotation per minute
SEM	Scanning electron microscope
TEM	Transmission electron microscopy
USP	Ultrasonic Spray Pyrolysis
UV-Vis-NIR	Ultraviolet-Visible Near Infrared
VOPcPhO	Vanadyl 2,9,16,23-tetraphenoxy-29H,31H phthalocyanine
XPS	X-ray photoelectron spectroscopy
XRD	X-ray Diffraction

CHAPTER 1

INTRODUCTION

The unique properties of nanostructured materials have generated great interest among researchers. It is due to the decreasing scale of device and the interesting optical properties associated with nano size of particles, since the optical properties can be tuned by quantum confinement effects at nano sizes [1]. There are numbers of fabrication methods of nanostructured materials such as sol-gel, Micelle and inverse Micelle, hydrothermal, electrodeposition, ultrasonic spray pyrolysis (USP), sonochemical and template-assisted method [2-16]. Among all of the existing methods, template-assisted method is claimed to be the most cost effective and superficial fabrication technique.

This research has been motivated from the unique properties possess by VOPcPhO in particular its metal phythalocyanine that able to improve light absorption within the solar spectrum [17, 18]. Phythalocyanine is reported to be a great material in optoelectronic devices considering that it is capable to exhibit the intense absorption mainly in UV-vis spectral region [19, 20].

The overall goal of this work is to assess the potential of template-assisted method for the fabrication of novel nanostructured materials. There are two main objectives in this work (i) to fabricate the VOPcPhO nanoflowers and (ii) to fabricate the P3HT:VOPcPhO composite nanorods. The morphological, structural and optical properties of these nanostructures are studied by varying its solution concentration, spin coating rate and annealing temperature.

This research report is organised in the following manner. Chapter 1 provides the objectives of the research, motivation of research focus and an overview throughout the contents of this report. Chapter 2 explains the relevant review that related to the fabrication of nanostructured materials. Chapter 3 focuses on the methodologies relevant to the overall work. The variation of parameters such as the solution concentration, spin coating rate and annealing temperature will be explained in details. These parameters and methodologies are essential to the readers' full understanding of the method.

Chapter 4 presents the results and discussion of the overall studies which includes the morphological, structural and optical properties of nanostructured materials. It contains the details of process parameters and discusses the factors responsible to the growth mechanism. Finally, Chapter 5 is the conclusion of the dissertation work.

CHAPTER 2

LITERATURE REVIEW

2.1 Nanotechnology and Nanomaterial

Nanomaterials should have fulfilled the two conditions which the first one is at least one of dimensions is nano and some properties of these materials are specific to the nano dimension. Nanostructured materials can exist in many forms such as nanocomposites, nanocapsule, nanoporous, nanoflowers, nanofibres, nanowires and nanotubes [2, 21-24]. The biggest challenge in nanotechnology is to synthesis the nanostructured materials since they exhibit small size and complexity of nanoscale structures [25]. A number of different techniques have been reported in order to synthesis nanostructured materials aiming to control their size, morphology, structure and chemical composition [26, 27]. Today, nanomaterials have been inspiring a great amount of interest due to the major breakthroughs of the discovery of bucky balls and carbon fullerene structures (Noble prize), the first electron microscope images of carbon nanotubes, and the invention of inorganic fullerenes and anisotropic nanostructures [28, 29]. A large number of reviews and researches regarding nanotechnology have been published, making nanotechnology as ground-breaking topics in today's science and technology [30-32]. Changes in dimension of materials can contribute to the dramatic changes in physical and chemical properties of nanomaterials. For instance, the change of material's dimensions (within the length range of quantum confinement) could results to the changes of the total energy and the occupation of the outermost energy level [33]. This phenomenon explained the fascinating of nanostructured materials compared to their bulk counterparts.

2.2 Template-Assisted Method

Template-assisted method provides a convenient and versatile method in the fabrication of nanostructured materials. In this method, a template with small nano-sized pores provides a platform for nanostructures growth in the way that desire materials filling and replicate the template's pores structure. Almost every materials can be employed in template-assisted method resulting in a structure such nanowires [34-36], nanorods [22, 37], nanotubes [38, 39], and nanoflowers [21]. In details, the template can be readily used as a supporting matrix without any further fabrication process. The template is defined as a hard template such as anodic aluminum oxide (AAO) membrane, nanochannel glass (NCG) and porous polymer membranes in which the template contains nanoscale channels within the host material [37-41].

AAO templates have attracted numerous considerations as a tool in the fabrication of nanostructured materials due to its simplicity and economical [43-45]. Studies show that alumina exhibits porous structure under certain electrochemical anodization conditions [46, 47]. There is a number of electrolyte systems and a wide range of concentrations along with different temperatures and anodization regimes have been studied. A small pore diameter of about 6 - 10 nm has been reported by using a sulfuric acid solution [48]. Lira et al. claimed that 5 nm pore size can be obtained by applying electrical pulses at the end of general PAA fabrication process [49]. However, an ultrasmall pore size tends to have an unparalleled orientation [50].

In conjunction with that, the different mechanisms have been proposed to describe the formation process of the self-ordered hexagonal pore array [51, 52]. Fabricating nanopore arrays of alumina are one of the well-established processes nowadays and even commercially available from Whatman Anodisc. The fabrication of nanostructured materials via template-

assisted method can be realised by numerous depositions such as sol-gel, dip-coating method, electrochemical deposition and chemical vapour deposition [53-58]. Nanostructures are released from the templates by dissolving the porous alumina template with NaOH [21].

2.2.1 Electrochemical Deposition

Fabrication of nanostructured materials using electrochemical deposition into the nanopores of anodic aluminum oxide (AAO) membranes has create a huge scientific interest for its outstanding features exhibited by these templates such as low cost, large self-ordering degree of nanopores, high reproducibility and precise control over their morphological characteristics [59]. In this technique, the combined bottom-up strategies allow the fabrication of nanomaterials by electrochemically filling the template pores. The amount of electrodeposited material can be easily controlled through the charge recorded during the nanomaterials growth [60]. This phenomenon resulting in the ability of formation of highly ordered nanostructures with specific dimensions and properties. Through this technique, AAO template is coated with a metallic conductive layer which acts as a cathode for electrodeposition. Then a voltage is applied between the cathode and anode. The cations in the electrolyte solutions will be attracted to the cathode and get reduced. The growth of nanowire will happen inside the template's pores. The length of the nanowires depends on the length of the nanochannels, the electrodeposition duration and the thickness of the template. The AAO template-assisted method has been proved to be a well-controlled approach to fabricate the ordered inorganic nanomaterial arrays with narrow diameter distribution. Diameter of the nanomaterial arrays is limited by the pore size of the template which can be further controlled by the anodization conditions and the wet etching steps after anodization.

Different varieties of nanostructures such as nanowires, nanotubes and nanorods can be obtained via template-assisted method [60-63].

2.2.2 Sol-Gel Deposition

The sol-gel process involves the transition of a system of colloidal particles (the sol) into a solid phase (the gel). First, the hydrolysis of a solution of precursor molecules forms a suspension of colloidal particles. Then the templates are immersed into the solution and the condensation of the colloidal particles within the nanochannels yields a new gel phase [38, 55-57]. Finally, the post heat treatment turns the gel phase into solid nanostructures with good crystallinity. The main advantages of sol-gel techniques include the low processing temperature, versatile and straightforward. Metal oxide nanowires (VO_2 [56], ZnO [62], TiO2 [63]) and element nanowires (Zr,Ti [64]) have been synthesized using sol-gel deposition method.

2.2.3 Dip-coating Deposition

The dip-coating process is similar to sol-gel deposition except that the template is put into a precursor solution instead of the sol solution [65]. Silver nanotubes are synthesized by dipping the AAO template in $AgNO_3$ solution followed by drying, thermal decomposition, and subsequent dissolution of the AAO template [66].

2.3 Donor Materials (*p-type*)

2.3.1 Poly(thiophene)

Poly(thiophene) (PT) is one type of conjugated polymer that offer a very useful physical and electrical properties in term of its solubility, charge mobility, electrical and conductivity [68, 69]. Certain properties of PT can be controlled by chemical modification. Generally, the formation of poly(thiophene) started from the polymerization of thiophene monomers with sulphur heterocycle that has an ability to become conducting through doping process where electron either been added or removed from conjugated π-orbitals. Figure 2.1 shows the chemical structure of monomer repeating unit of PTs.

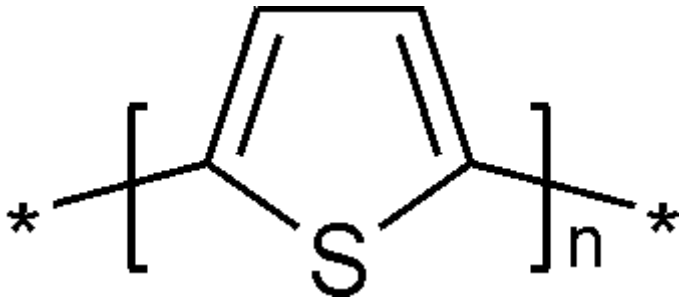

Figure 2.1: Chemical structure of monomer repeating unit of PTs

Since early 1981, there are numbers of researches and reviews on PTs that have been reported [70-76]. A comprehensive and detailed review on PTs has been published by Schopf and Koβmehl in 1997 [76]. In 1992, Roncali reported on the electrochemical synthesis [71] and in 1997 the electronic properties of substituted PT was reported [72]. Studies have shown that polythiophene are thermally and environmentally stable [73, 74]. Researchers have doped polythiophene and/or its derivatives with $FeCl_3$, iodine [75], Bu_4NClO_4, Et_4NBF_4, Et_4NBF_6 [71], and VOPcPhO [22, 76] since PT can be chemically modified via doping with acceptor materials.

2.3.2 Poly 3-hexylthiophene-2,5-diyl (P3HT)

The chemical structure of P3HT is shown in Figure 2.2. P3HT has a very unique optoelectronic properties as P3HT possess the highest charge carrier mobility compared to others conjugated polymers and its hole mobility is reported as high as 0.1 $cm^2V^{-1}s^{-1}$ making P3HT as one of the most promising materials as electron donor [78]. The remarkable charge mobility of P3HT is due to its ability to self-organize into ordered lamellae that caused strong interchain interactions hence increasing the efficient charge transport between the polymer chains. Furthermore, studies shows that P3HT has a high chemical stability and low optical band gap of 1.9-2.0 eV that matches the strongest sunlight [79]. However, pure P3HT based devices may have a limitation for the broad absorption profile to collect as much photons in the range of solar spectrum especially in the ultra violet region [80]. Highest occupied molecular orbital (HOMO) level of P3HT will limit the maximum open circuit voltage which causes oxidation instability of pure P3HT devices under ambient condition [81]. One of the ways to reduce the limitation of P3HT is via blending with inorganic nanoparticles.

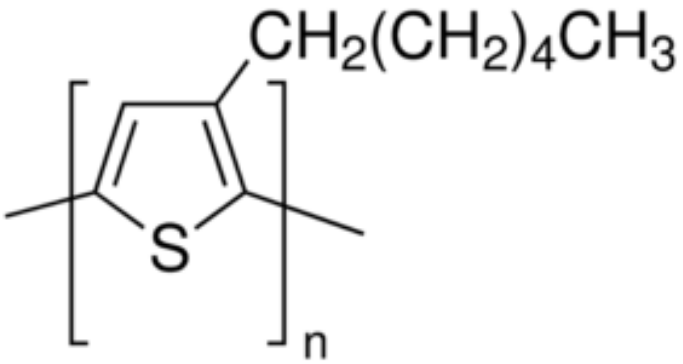

Figure 2.2: Chemical structure of P3HT

2.4 Acceptor Materials (*n-type*)

2.4.1 Vanadyl 2,9,16,23-tetraphenoxy-29H,31H-phthalacyanine (VOPcPhO)

Coordination complex also known as metal complex is consist of an atom or ion which usually metallic, and its surrounding by bound molecules which act as ligands or in other words a complex agents. Mostly metal-containing compounds majority the transition metals consist of coordination complexes [82]. Study shows metal phthalacyanine have widely used as catalyst in redox reactions. The research attraction is the oxygen reduction reaction of gas stream by removing hydrogen sulfide. It has been proven that phthalacyanine can act as an acceptor material in organic solar cell [83]. Metal phthalacyanine have a unique characteristic which it is able to improve absorption of the solar spectrum [84, 85]. Phthalacyanine are believed to be a great material in optoelectronic devices as they exhibit a very intense absorption especially in UV-Vis spectral region [86, 87]. VOPcPhO has been studied for its photovoltaic properties especially in organic solar cell due to its high solubility in most of the organic solvent. In the photovoltaic applications, VOPcPhO act as an active layer of a single thin layer in where the electron-hole separation takes place. A number of fabrication method is available to synthesis VOPcPhO thin layer such as reprecipitation method, chemical vapour deposition and spin coating techniques [21, 88, 89]. In addition, VOPcPhO is a low molecular weight organic semiconductor which has a low series resistance and has a relatively high mobility for a single component film [75, 88]. From Figure 2.3, it can be observed that metal phthalocynine consist of vanadyl as a core center atom and it is surrounding by four isoindole units.

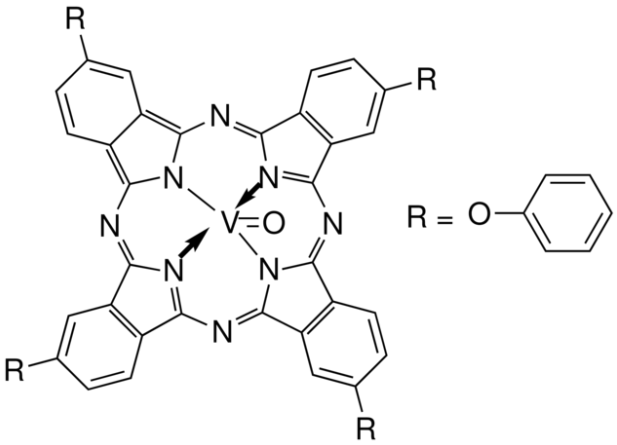

Figure 2.3: Chemical structure of VOPcPhO

CHAPTER 3

METHODOLOGY

3.1 Overview

As been discussed in the previous chapter, template assisted-method tends to be one of the most costs effective and familiar methods [89]. This chapter describes the methodologies used in this work. The goal in providing this detail is to give the reader an understanding of the technique used to synthesis the nanostructured materials. Several parameters have been fixed to study the growth mechanism of the nanostructures and its optical properties.

3.1.1 Alumina Porous Template

High aspect ratio alumina porous template with diameter of 20 nm and 60 μm in thickness were purchased from Whatman (Figure 3.1). These templates can withstand temperatures of 600 °C.

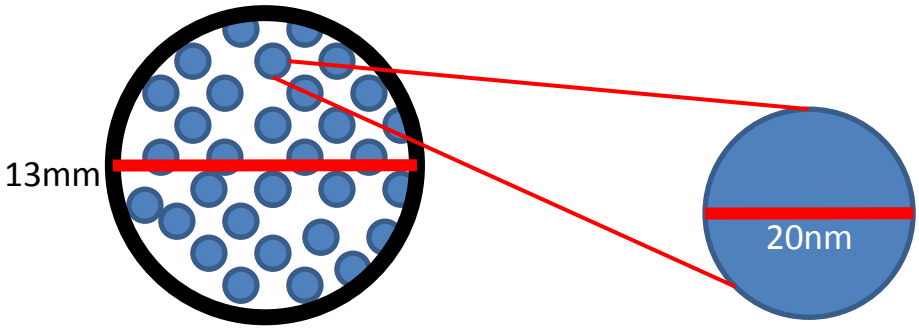

Figure 3.1: Plane view of porous alumina template

In order to keep the porous of the template free from any impurities, the templates were first underwent a cleaning process by sonicating in acetone for 15 minutes followed by sonicating in distilled water for another 15 minutes and let it self-dry in room temperature.

3.1.2 Materials Preparation

Materials (VOPcPhO and P3HT) bought from Sigma-Aldrich were used without further purification. 5 mg/ml of P3HT that has been dissolved with chloroform was prepared for the fabrication of composite nanorods. In order to study the effect of solution concentration on VOPcPhO nanoflowers growth, two different solution concentrations (5 and 15 mg/ml) of VOPcPhO were prepared.

3.1.3 Experimental Parameters

Several parameters were set in order to study the difference in morphology and optical properties due to solution concentration, spin coating rate and annealing temperature. Two different solution concentrations of VOPcPhO were prepared with chloroform which is 5 mg/ml and 15 mg/ml. The second parameter is the spin coating rate which were set at 1000 rpm and 2000 rpm. The annealing process was done in a furnace for 15 minutes and its temperatures were set at 50^{o}C and 150^{o}C. All the experimental parameter can be summarized in Table 3.1.

Table 3.1: Experimental parameter for synthesis of VOPcPhO nanoflowers

Solution Concentration (mg/ml)	Spin Coating Rate (rpm)	Temperature (^{o}C)	Label
5	1000	50	5 / 1000 /50
5	1000	150	5 / 1000 / 150
5	2000	50	5 / 2000 / 50
5	2000	150	5 / 2000 / 150
15	1000	50	15 / 1000 /50
15	1000	150	15 / 1000 / 150
15	2000	50	15 / 2000 / 50
15	2000	150	15 / 2000 / 150

3.2 Experimental Techniques

VOPcPhO nanoflowers and P3HT:VOPcPhO composite nanorods were prepared in this study. For the propose of reference, VOPcPhO thin films and P3HT:VOPcPhO composite thin films were prepared. Each of the mentioned samples and references has a different technique of preparation which will be discussed in details.

3.2.1 Preparation of Vanadyl 2,9,16,23-tetraphenoxy-29H,31H Phthalocyanine (VOPcPhO) Nanoflowers

Clean alumina porous template was placed on top of the spin coater and VOPcPhO solution with different concentration of 5 and 15 mg/ml was dropped cast on top of the template, then immediate spin coat was applied at two different rates of 1000 and 2000 rpm. The template and VOPcPhO layer on top of it then underwent an annealing process at two different temperatures which were 50^{o}C and 150^{o}C. The next step is to place a copper tape on top of the VOPcPhO layer and dissolve the template into sodium hydroxide, NaOH overnight. The final product will be a copper tape with VOPcPhO nanostructured on top of the copper tape. These steps can be briefly explained by Figure 3.2.

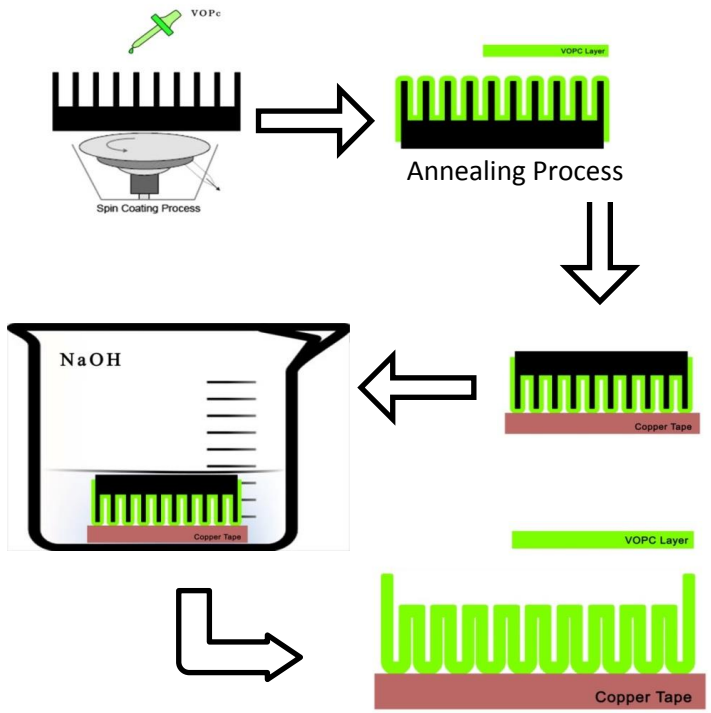

Figure 3.2: Schematic illustration of preparation of VOPc nanoflowers

3.2.2 Preparation of P3HT:VOPcPhO composite nanorods

Clean alumina porous template was placed on top of the spin coater and P3HT solution with a concentration of 5 mg/ml was dropped cast on top of the template, then immediate spin coat was applied at a rate of 1000 rpm. Then it will undergo an annealing process at 150 ^{o}C. VOPcPhO solution with a concentration of 5 mg/ml was then drop cast on top of the P3HT layer and once again immediate spin coat is applied at the rate of 1000 rpm. The template and P3HT:VOPcPhO layer on top of it then underwent an annealing process at 150 ^{o}C. The next step is to place a copper tape on top of the P3HT:VOPcPhO layer and dissolve the template into NaOH overnight. The final product will be a P3HT:VOPcPhO composite nanorods. These steps can be briefly explained by Figure 3.3.

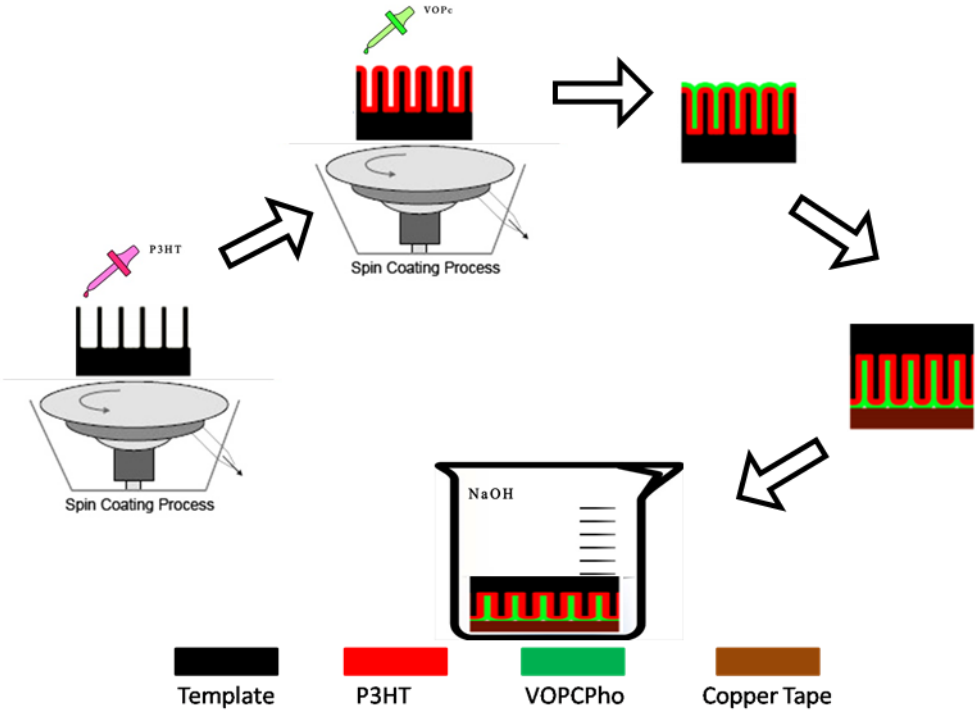

Figure 3.3: Schematic illustration of preparation of P3HT:VOPcPhO composite nanorods

3.2.3 Preparation of VOPcPhO thin films

VOPcPhO thin film was synthesised as a reference. Clean glass was used as a substrate. Two different concentrations of VOPcPhO solution, 5 mg/ml and 15 mg/ml were drop cast on top of the clean glass and immediate spin coat was applied at two different rates of 1000 rpm and 2000 rpm. The glass and VOPcPhO layer on top of it then undergo an annealing process at two different temperatures of 50 ^{o}C and 150 ^{o}C. These steps can be briefly explained by Figure 3.4.

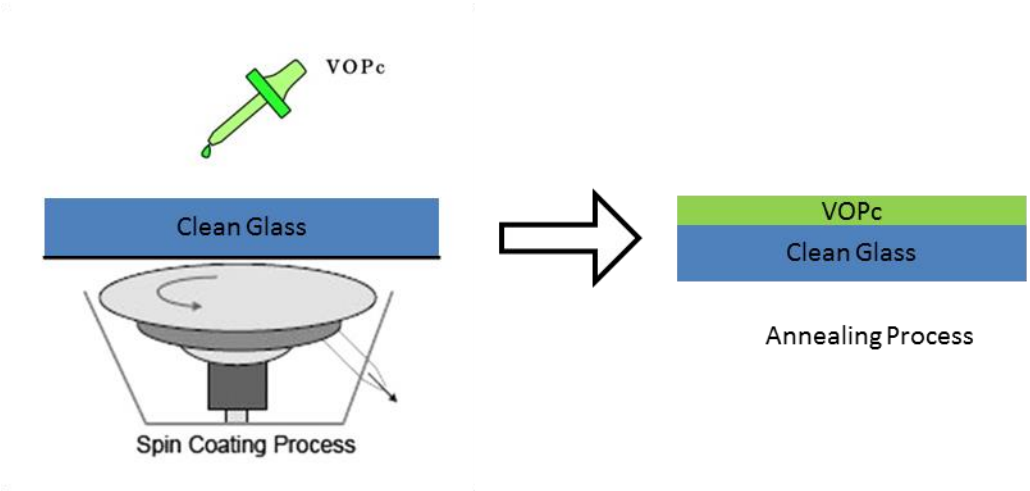

Figure 3.4: Schematic illustration of preparation of VOPcPhO thin films

3.2.4 Preparation of P3HT:VOPcPhO composite thin film

P3HT:VOPcPhO composite thin film was synthesised as a reference. Clean glass was used as a substrate. P3HT with solution concentration of 5 mg/ml was drop cast on top of the clean glass and immediate spin coat was applied at rate of 1000 rpm. Then it will undergo an annealing process at 150 ^{o}C. VOPcPhO with a solution concentration of 5mg/ml was then drop cast on top of the P3HT layer and once again immediate spin coat is applied at the rate of 1000 rpm. The glass and P3HT:VOPcPhO layer on top of it then undergo an annealing process at 150 ^{o}C. These steps can be briefly explained by Figure 3.5.

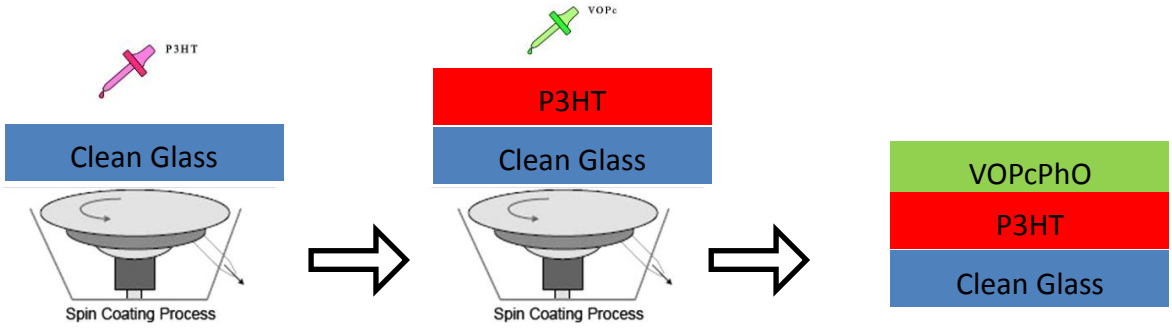

Figure 3.5: Schematic illustration of preparation of P3HT:VOPcPhO thin films

3.3 Characterization Techniques

In this study, a number of experimental techniques and instrumentation have been employed to characterize and investigate the morphological, structural and optical properties of VOPcPhO nanoflowers and P3HT: VOPcPhO composite nanorods as well as thin films.

3.3.1 Field-Emission Scanning Electron Microscopy (FESEM)

To study the morphological and structural properties of VOPcPhO nanoflowers and P3HT:VOPcPhO composite nanorods, samples have been characterised using FEG Quanta 450, EDX-OXFORD. Scanning electron microscope (SEM) is an electron microscope that able to produce an image of the materials from energetic electron beam that scan across the sample on a fine scale. The electron beam interact with the sample's atom resulting the signal generations that contains the sample's surface topography, composition, distribution pattern, shape, size dimension and the crystallographic features [90].

Several important parts in SEM consists of electron gun, electron beam, first condenser lens, second condenser lens, deflection coils, backscatter electron detector, vacuum pump, X-ray detector, objective lens and secondary electron detector. The structure of SEM can be described in Figure 3.6. The electron gun is fitted with tungsten filament cathode

because of its high melting point and low vapour pressure. An electron beam will be thermionically emitted from electron gun upon heating of the filament. The beam usually contains energy in the range of 0.2 to 40.0 keV is focussed to a spot about 0.4 to 0.5 nm in size by a number of condenser lenses. The beam will deflect to x and y axis once it passes through pairs of deflection coils in the electron column. Accordingly, a scanning in a raster pattern over a rectangular area of the sample surface can be performed. Upon interaction of the primary electron beam with the sample, the electron loses energy by continuous random scattering and absorption within the sample. The loss in energy from the electron beam produce reflections of highly energetic electrons by elastic scattering and emissions of secondary electrons by inelastic scattering. The beam that absorb by the sample can be detected and the signal is then being convert and amplified by electronic amplifier which enable to display an image as variations in brightness mode from the computer's monitor.

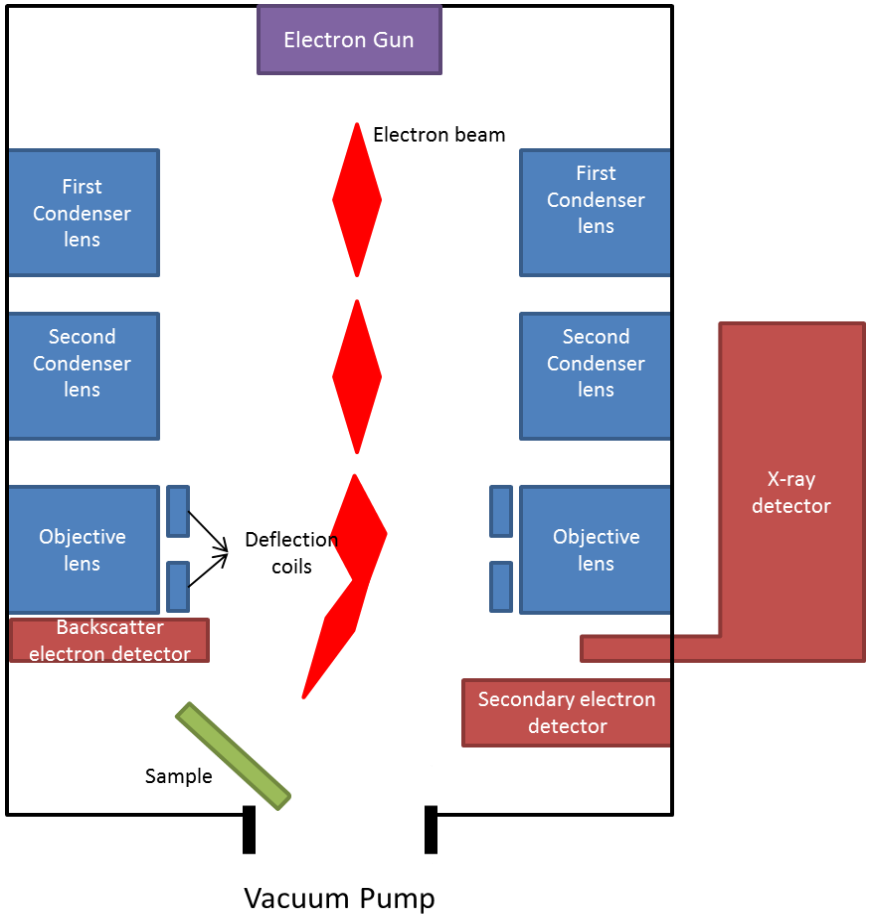

Figure 3.6: Principle features of SEM instrument

When it comes to Field-Emission Scanning Electron Microscopy (FESEM), several advantages are available compared to SEM. FESEM comprises of a field-emission cathode in the electron gun which able to generate narrower probing beam. FESEM has a capability in reducing the electrostatically distorted and producing a clearer image compared to SEM. Smaller contamination spot in the grain size can be examined in FESEM. Finally, compared to SEM, FESEM has a lower probability of sample damage because it has a lower penetration of electrons with low kinetic energy closer to the sample.

3.3.2 Transmission Electron Microscopy (TEM)

TEM is an instrument that capable of imaging the inside of a specimen directly at the atomic level (1, 500 000x or 1.5 million x). TEM has an extensive range of applications and handles a variety of specimens such as biological, metallic, mineral and ceramic specimens. TEM has a large focal depth so that the entire visual of a thins-section specimen can be brought into focus. Images from TEM are presented as a monochrome image and it is corresponding to the intensity of the electron beam. Basic principle of TEM, when the electron beam is projected through a specimen in a vacuum and the electron beam transmitted through the specimen provides a rich variety of information about the specimen. Among the signals from the specimen, transmitted electrons and elastically scattered electron are used mainly for TEM. The elastically scattered electrons are the ones that have transmitted through the specimen with a change in the forward direction which was caused by the interaction between the incident electron and an atom in the specimen. The inelastically scattered electrons are the ones that lose part of its energy due to its interaction with the electrons of an atom in the specimen during the course of transmission. Figure 3.7 shows the basic principle of TEM when electron beam is projected through the specimen.

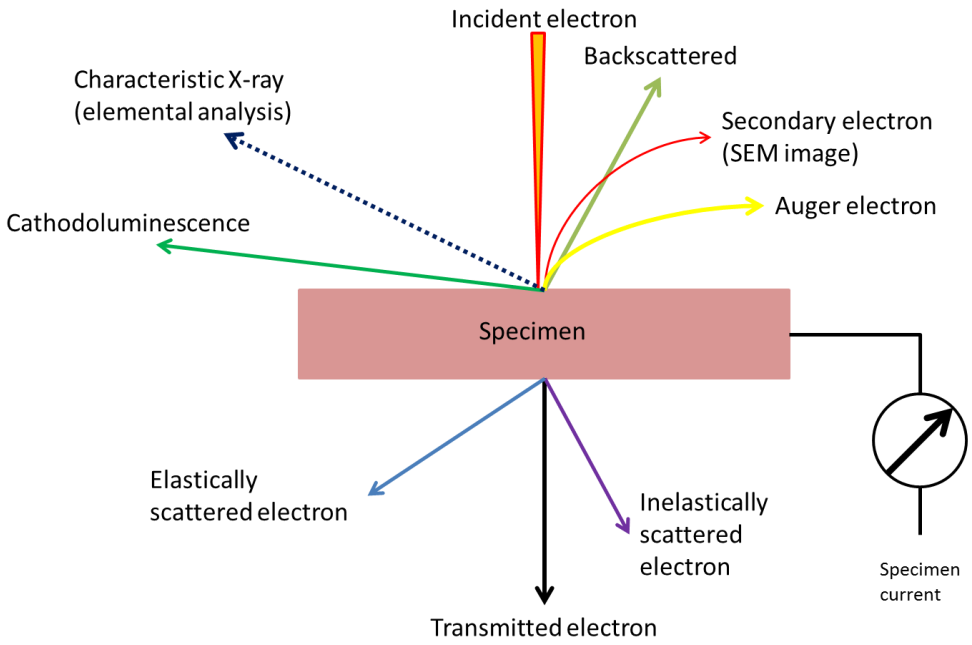

Figure 3.7: Basic principle of TEM when electron beam is projected through the specimen

Structure of TEM mainly consists of three primary systems including microscope column, evacuation system, high voltage transformer and power supply system. The microscope column section is the most important part in TEM as this system consists of five important sections which firstly is the electron gun where the generations of electron beams take place. Secondly is the illumination system lens section in which electron beam brightness and viewing area are controlled. Thirdly is the specimen chamber in which a specimen is placed and can be moved vertically/horizontally, rotated and tilted. Next is the imaging system lens section in which an image or electron diffraction pattern is magnified. Finally is the viewing chamber in which a magnified image or electron diffraction pattern is observed on a fluorescent viewing screen and recorded on film. Figure 3.8 shows the cross-sectional view of TEM. In this work, Technai G^2 20S Twin TEM is used to further study on the morphological and structural of VOPcPhO nanoflowers and P3HT:VOPc composite nanorods.

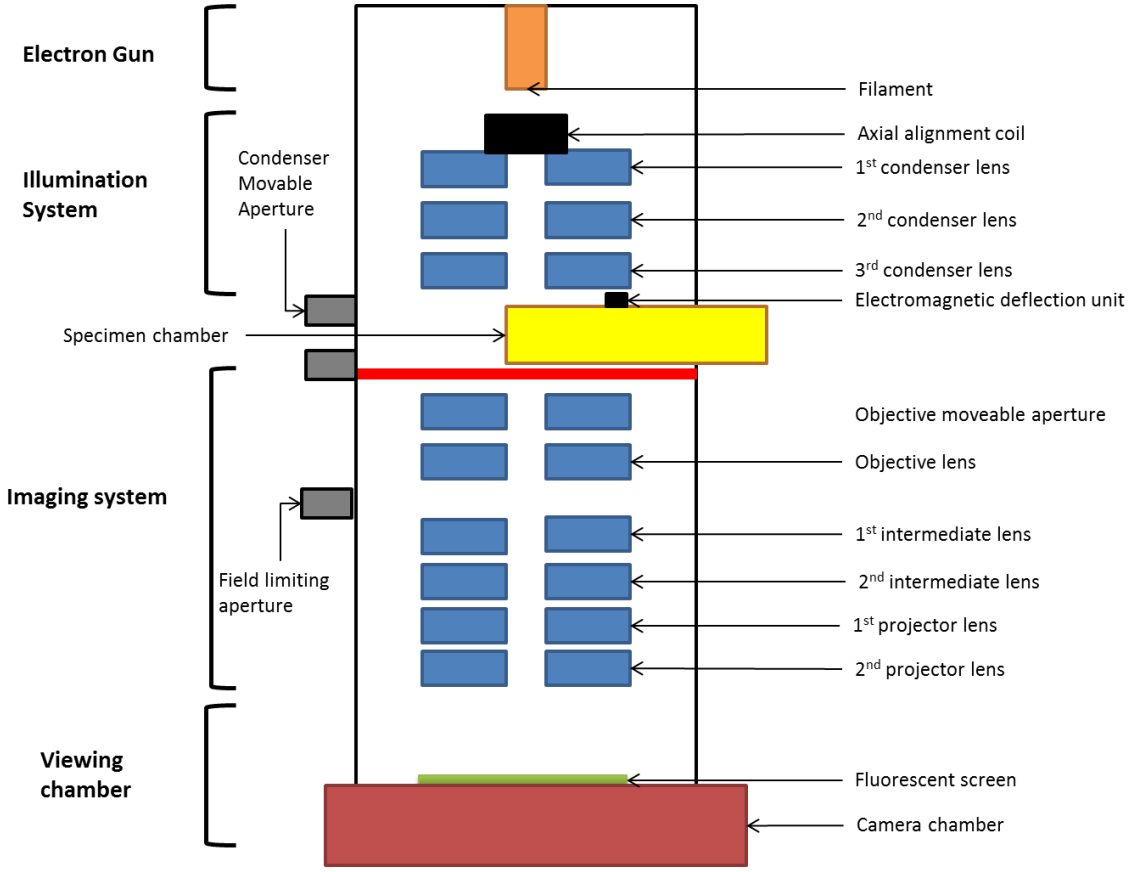

Figure 3.8: Cross-sectional view of TEM

3.3.3 Ultraviolet-Visible-Near Infrared (UV-VIS-NIR) Spectrophotometer

In general, the working principle of UV-vis spectroscopy involves the ability of the photons to be absorbed by the molecule in the UV-Visible region of the electromagnetic spectrum which contributes to a transition of electron from HOMO to LOMO level. There are several possible of electronic transition that molecule may experience involving π, σ or n electrons which include $\sigma \rightarrow \sigma^*$ transitions, $n \rightarrow \sigma^*$ transitions, $n \rightarrow \pi^*$ transitions and $\pi \rightarrow \pi^*$ transitions as shown in Figure 3.7.

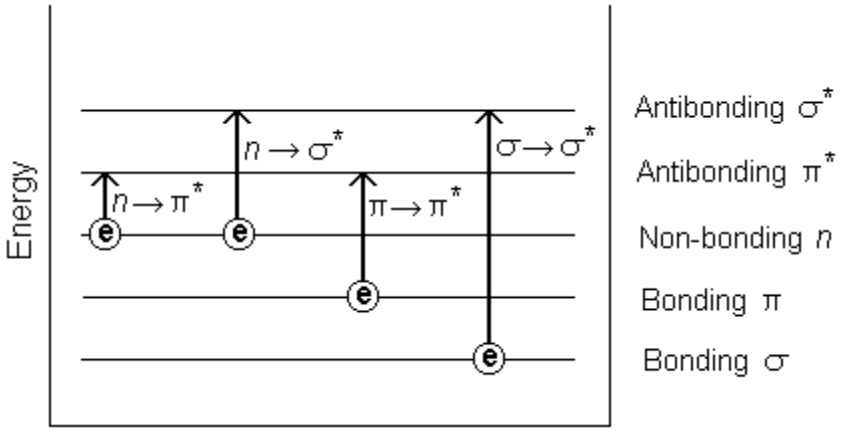

Figure 3.9 Possible electronic transitions of π, σ or n electrons

For organic materials, the absorption spectroscopy is mainly based on the transition of n or π electron from bonding state to π* excited anti bonding state (n→π*, and π→π* transitions), whereby the absorption peaks for these types of transition typically fall in the range between 200 to 800 nm (B.C. Course, 2011). Additionally, these transition require an unsaturated compound in the molecules to provide π electrons which is different from n → σ* transitions that is undergone by saturated compounds containing atoms with non-bonding free electrons. Both n → σ* and σ→ σ* transitions requires an absorption of photon with a shorter wavelength less than 200 nm. Hence, merely n→π* and π→π* transitions that take place at a longer wavelength in the UV-vis region are noticeable.

Generally, there are three main components in UV-Vis-NIR which include a light source, monochromator and detector. Light source consists of visible light and UV light source. Monochromator is used to pick the right light beam to a selective wavelength. Detector basically functions as an examiner of the light intensity. UV-Vis-NIR Spectrophotometer, model Jasco 570 UV-VIS/NIR was used in this study to obtain the UV-vis absorption spectra. There are two different types of light source used in Jasco 570 UV-VIS/NIR which is deuterium discharge that incident its light at ultraviolet region and secondly is tungsten iodine lamp that is used in visible and near infrared regions. Light source

will provide a light beam that directed to monochromator. The monochromator will choose the suitable light beam depended to the wavelength required at the certain time. The light is then split into two beams by a beam splitter which directed to sample and reference holders accordingly. Both beams examined using photodiodes detectors before it being amplified using the differential amplifier. Once the sample molecules are incident by light beam with an energy that matches a possible electronic transition, the molecules may favourably absorb part of the photon energy, hν. This will resulting to the excitation of the molecule from ground state, E_0 to the higher energy state, E_1 where we can defined $h\nu=E_1-E_0$. The absorption of the photons at a certain wavelength will be recorded and process by the computer software and will be available for display through computer monitor. The measurement setup for the UV-Vis-NIR Spectrophotometer in Table 3.2

Table 3.2: The measurement setup for the UV-Vis-NIR Spectrophotometer

Photometric Mode	A
Response	Fast
Band Width	5 nm
Scanning Speed	2000 nm/min
Start Wavelength	250 nm
End Wavelength	850 nm
Data Pitch	5 nm

3.3.4 Raman Spectroscopy

The optical properties of VOPcPhO and P3HT:VOPcPhO on Raman spectroscopy have been carried out using RENISHAW inVia Raman Microscope. Raman spectroscopy is able to provide the number of information including the information about the structure of molecule for both organic and inorganic materials. Through Raman spectroscopy the chemical identity and crystallinity of materials can be determined. It is also be able to detect stress in a semiconductor materials or devices [91].

Figure 3.8 shows the theory of Raman Effect. Once a sample is irradiated with a beam from intense monochromatic light source which usually a laser, most of the radiation from the light source will be scattered by the sample at the same wavelength as the incoming light also known as Rayleigh scattering. Only a small number of the incoming light is scattered at a wavelength that is shifted from the original light wavelength known as Raman scattering. Stokes Raman scattering happens whenever the incident photon gives energy to the sample. Anti-stokes Raman scattering is when the incident photon absorbs energy from the sample.

Molecule at the ground vibrational and electronic states said to be at rest resides. When the photons from the light source enter the system, it raises the energy of the system for an instant by inducing a polarization in the chemical species. The polarized condition is not a true energy state and is referred to as a ‘virtual state’. Relaxation from the virtual state occurs almost instantaneously and is predominantly to the initial ground state. This process produces Rayleigh scattering which the scattered light of the same wavelength as the excitation laser. Relaxation to the first excited vibrational level results in a Stokes-Raman shift. Stokes-Raman shift scattered light is of lower energy than that of the laser light. In most of the system, there must have at least a small population of molecule which at an excited vibrational state initially.

There are two types of Raman spectroscopy which is Dispersive Raman Spectroscopy and Fourier Transform Raman Spectroscopy. In this work, Dispersive Raman Spectroscopy, RENISHAW inVia Raman Microscope was used. Dispersive Raman spectroscopy is accomplished by focusing the Raman scattered light onto a diffraction grating, which split the beam into its constituent wavelength. These are directed into charged coupled device (CCD) detector. Typically, Dispersive Raman uses laser wavelength of 780 nm, 633 nm, 532 nm and 473 nm. The intensity of Raman scatter in Dispersive Raman is proportional to$1/\lambda^4$, hence a short excitation laser wavelength will result in stronger Raman signal. Diffraction grating dispersion and optical design of the spectrograph determine the spectral resolution which controlled the amount details that can be seen in the spectrum. The higher number of grating lines per unit leads to broader dispersion angle and higher spectral resolution will be obtained. The measurement setup for Raman spectroscopy used in this work is tabulated in Table 3.3.

Table 3.3: The measurement setup for the Raman Spectroscopy

Laser Source	516 nm
Lowest Wavelength	200 nm
Highest Wavelength	3200 nm
Laser Power	1.0 %

CHAPTER 4

RESULTS AND DISCUSSION

4.1 Morphological and Structural Properties

The morphological and structural properties of VOPcPhO nanoflowers and P3HT:VOPcPhO composite nanorods are studied via Field-Emission Scanning Electron Microscopy (FESEM) and Transmission Electron Microscopy (TEM).

4.1.1 VOPcPhO nanoflowers

As shown in Figure 4.1, VOPcPhO nanoflowers can be obtained after the dissolution of template in NaOH. VOPcPhO nanoflowers consist of a group of rosette which is long, spear-shaped, propagated and has a sharp end. The formation of VOPcPhO nanoflowers explained that VOPcPhO solution does not fully replicated the structure of the template as expected which to be in nanorods or nanotubes. The significant difference for the structured obtain compared to the template would be in its diameter of the VOPcPhO tubular. From the FESEM images, the diameter of VOPcPhO is recorded to be 500 nm in average; however, the pores diameter of the alumina porous template is only 20 nm. A tremendous different in the diameter size should highly associated due to the dissolution process of alumina porous template into NaOH. VOPcPhO may have absorbed the Na particle originated from NaOH hence expand the diameter of VOPcPhO. Osmosis process could happen during the dissolution process where the spontaneous net movement of solvent molecules (Na) could partially penetrate template [92]. This effect can be supported through EDX spectrum as in Figure 4.2 where Na has been one of the major compositions in the VOPcPhO nanoflowers.

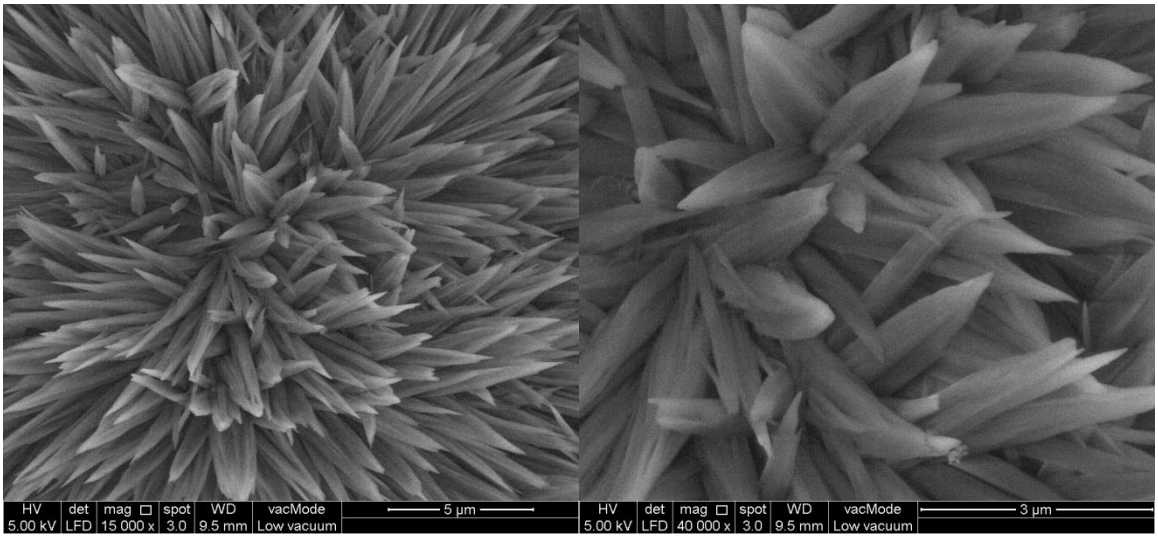

(a) (b)

Figure 4.1: FESEM images of VOPcPhO nanoflowers at (a) 15000x magnification and (b) 40000x magnification

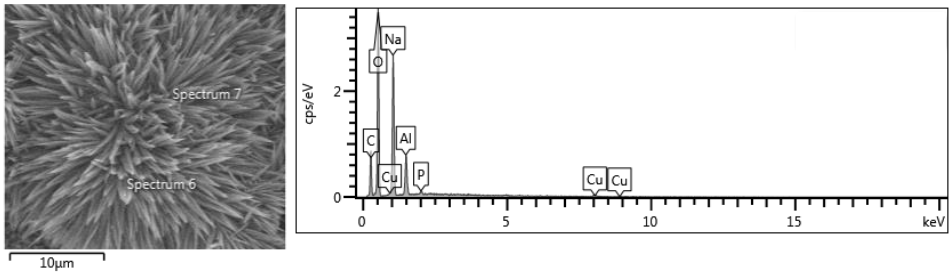

Figure 4.2: EDX Spectrum of VOPcPhO nanoflowers

The studies on morphology of VOPcPhO nanostructures continue using TEM images. From TEM images, close up images for individual rosette of the nanoflowers are shown in Figure 4.3. The formation of the rosette which has a spear-shaped and sharp end is due to the low infiltration rate of VOPcPhO solution into the alumina porous template. As the VOPcPhO does not fully infiltrate into the pores of the template, VOPcPhO tend to form a sharp end as shown in Figure 4.4. The formation of VOPcPhO nanoflowers can be illustrated in Fig 4.4. Once the VOPcPhO solution is dropped onto the template, the annealing process is carried out in order to increase the infiltration rate of VOPcPhO into the template's pore. Figure 4.4 (a) shows the VOPcPhO has infiltrated into a template after the annealing process is applied at 150 ^{0}C. The protruding tips are observed to grow within the template's pores.

Copper tape is attached on top of VOPcPhO before the removal of the template is done as in Figure 4.4 (b). Once the templates are dissolved into NaOH, the bottom part of VOPcPhO tends to shrink and self-assembly at one focal point which result to the structure of nanoflowers that shown in Figure 4.4 (c).

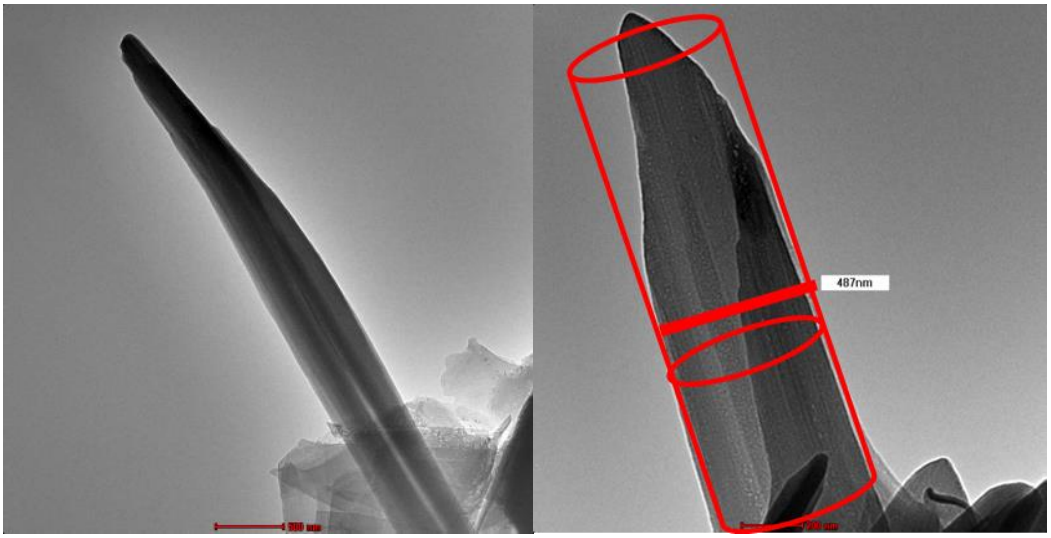

Figure 4.3: TEM images of rosette of VOPcPhO nanoflowers

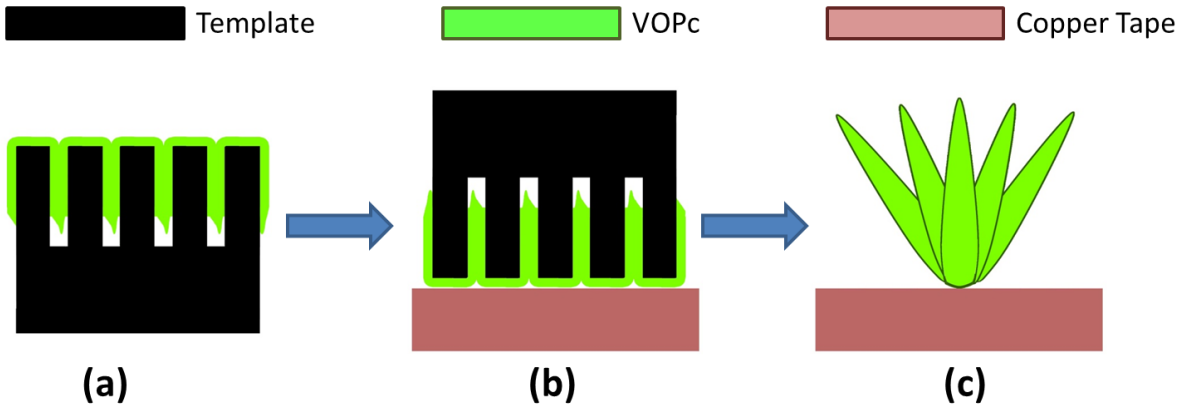

Figure 4.4: Schematic illustration of the formation process of VOPcPhO nanoflowers

The total of eight samples of VOPcPhO nanoflowers have been prepared and characterized for their morphologies. All of the samples have a difference in solution concentration, spin coating rate and annealing temperature, hence the effect of those differences on the morphological properties can be studied. Table 4.1 shows the FESEM images of all the eight different samples of VOPcPhO nanoflowers.

Table 4.1: FESEM images for VOPcPhO nanoflowers

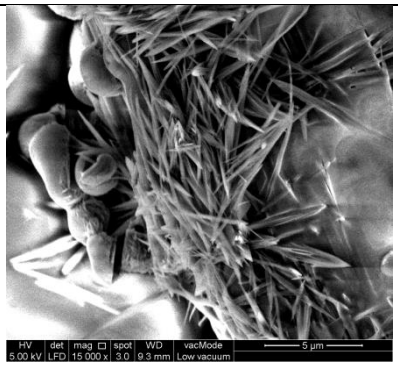 5/1000/50	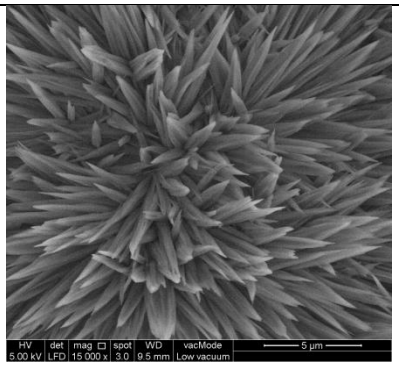 5/1000/150
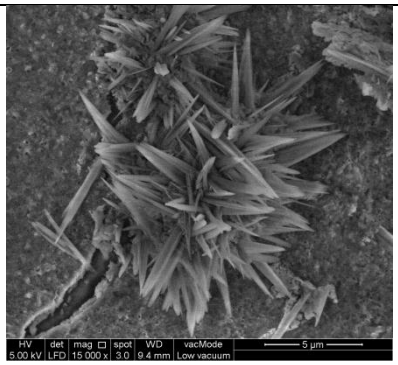 5/2000/50	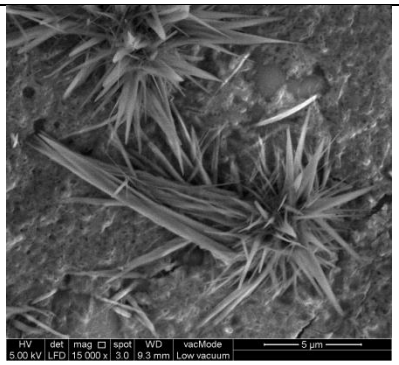 5/2000/150
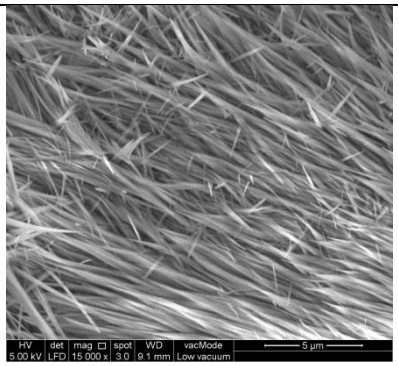 15/1000/50	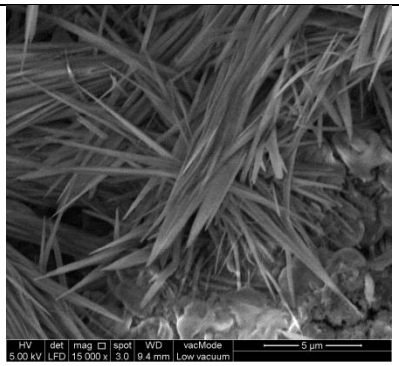 15/1000/150
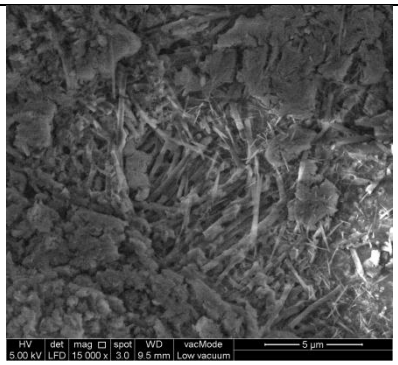 15/2000/50	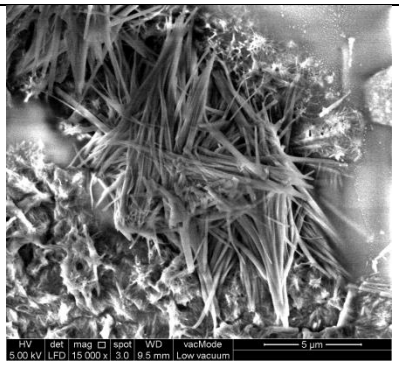 15/2000/150

From Table 4.1 it can be observed that the solution concentration, spin coating rate and annealing temperature is a control factor for the growth mechanism of VOPcPhO nanoflowers. However, it is obvious that the solution concentrations show a major aspect in controlling the structure of VOPcPhO nanoflowers. Two different concentrations of VOPcPhO used in this work are 5 mg/ml and 15 mg/ml. The structure of VOPcPhO with solution concentration of 5 mg/ml happened to form nanoflowers consist of standing rosettes. However, when the solution concentration increased to 15 mg/ml, the structure obtained consist of long collapsed nanostructures with a sharp end. Figure 4.5 explained the formation of nanostructured VOPcPhO of 15 mg/ml.

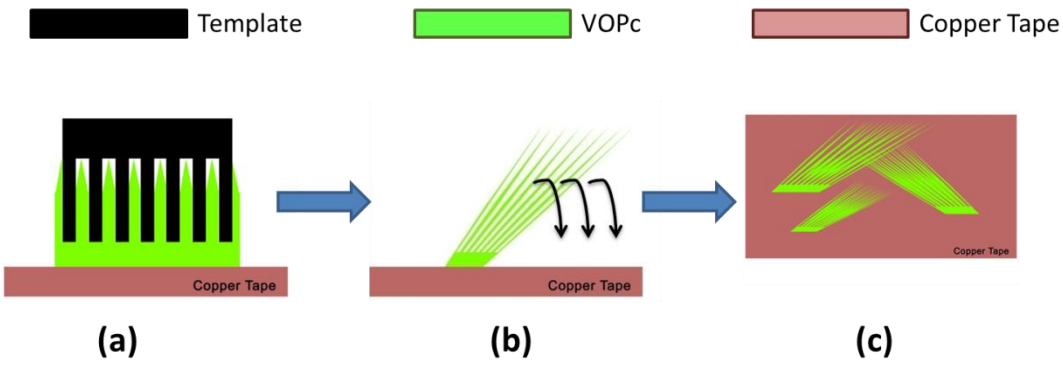

Figure 4.5: Schematic illustration of the formation process of VOPcPhO nanostructured for solution concentration of 15 mg/ml

The illustration from Figure 4.5(a) shows that higher solution concentration contributes to a better infiltration rate. Higher infiltration rate results to the longer tubular-shaped nanostructures almost twice a length compare to the standing rosettes. Figure 4.5 (b) shows the schematic diagram of tubular-shaped VOPcPhO losing its support and it tends to collapsed onto the copper tape as shown in Figure 4.5 (c).

4.1.2 P3HT:VOPcPhO composite nanorods

P3HT:VOPcPhO composite nanorods can be observed after the dissolution of alumina porous template with NaOH. Figure 4.6 (a) and (b) show the FESEM images of P3HT:VOPcPhO composite nanorods obtain from VOPcPhO solution concentration of 5 mg/ml. It can be observed that the composite consists of the array of nanorods. The nanorods have been successfully replicated from the template's pores. A low solution concentration of 5 mg/ml of P3HT has led to a low viscosity which allows the solution to infiltrate into the template's pores effortlessly. Enhancement on infiltration rate can overcome the interfacial issue between P3HT and VOPcPhO composite.

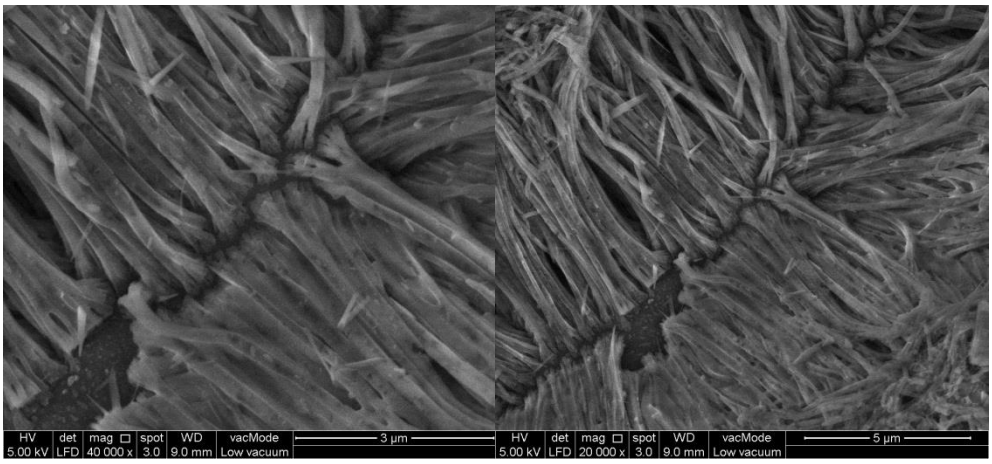

(a) (b)

Figure 4.6: FESEM images of P3HT:VOPcPhO composite nanorods at (a) 40000 and (b) 20000 magnification

The structural properties of P3HT:VOPcPhO composite nanorods can be further substantiated from the TEM images. Figure 4.7 shows an individual tubular nanotube of P3HT. It can be observed that P3HT nanotube have a rod-shaped of regular wall. Infiltration of VOPcPhO into P3HT nanotube has been successfully completed which further proven by the TEM images of P3HT:VOPcPhO composite nanorods in Figure 4.8. It is clearly shown

that the nanorod consists of inner and outer region. The outer region which is the brighter region corresponded to P3HT layer which act as a shell with a thickness approximately 20 nm. The nanorod composite obviously has a solid inner core which can be found at the darker region that corresponds to the VOPcPhO layer. The appearance of visible domains of molecules aggregation and arrangement in Figure 4.8 suggested that the solid inner core can be identified as VOPcPhO [21].

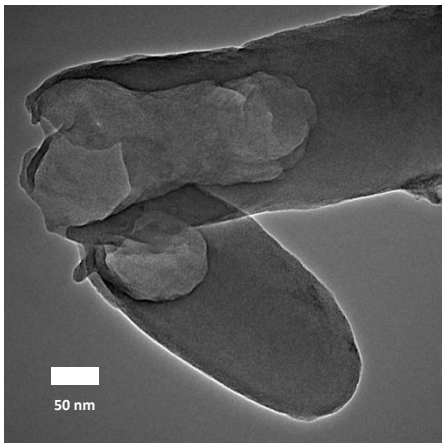

Figure 4.7: TEM image of individual tubular nanotube of P3HT

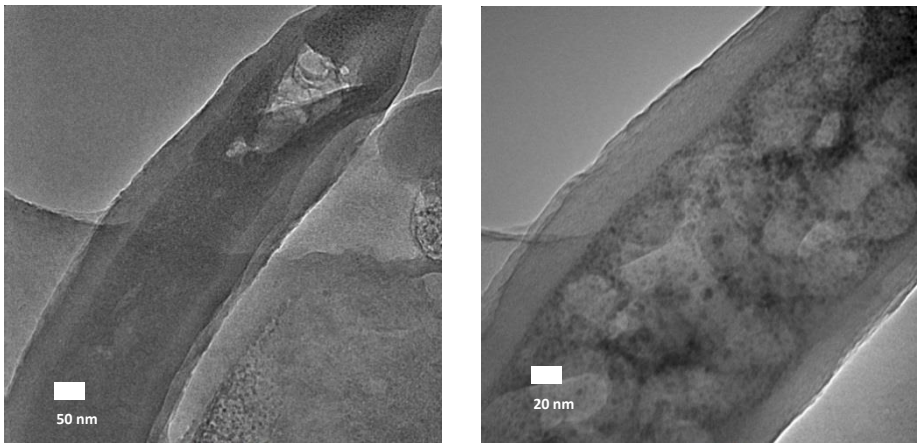

(a) (b)

Figure 4.8: TEM images of P3HT:VOPcPhO composite nanorods

Figure 4.9 shows the EDX spectrum of P3HT:VOPcPhO composite nanorods. The composition of P3HT:VOPcPhO composite nanorods consists of carbon (C), oxygen (O), sodium (Na), aluminium (Al), copper (Cu), vanadium (V) and sulphur (S). EDX spectrum acquired from composite nanorods exhibits peak of vanadium and sulphur which assigned to VOPcPhO and P3HT, respectively.

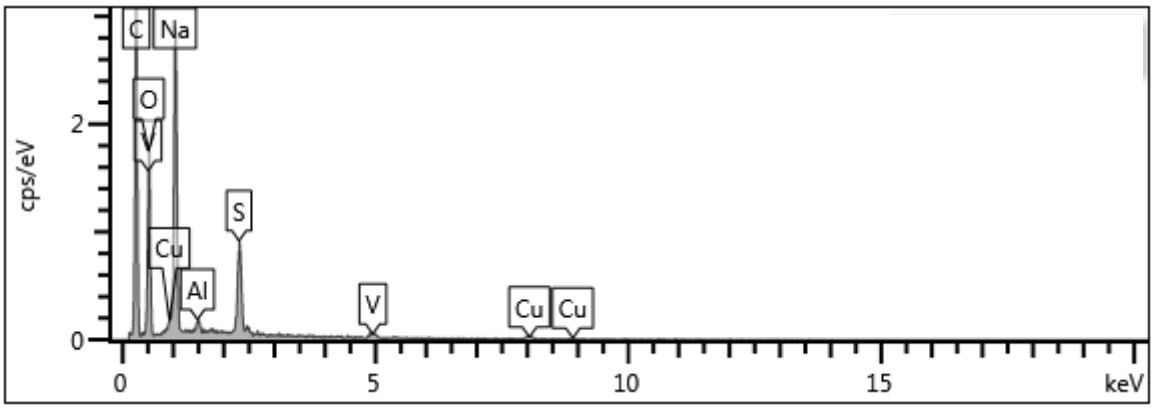

Figure 4.9: EDX spectrum of P3HT:VOPcPhO composite nanorods

The formation of P3HT:VOPcPhO composite nanorods can be illustrated as in Figure 4.10. The alumina porous template was cleaned in order to ensure the pores of the template free from any impurities (a). P3HT has been infiltrated into the template pores after the annealed process at temperature of 150 ^{0}C (b). VOPcPhO was deposited on top of P3HT via spin-coated and the infiltration of VOPcPhO can be observed (c). Copper tape is attached on top of P3HT:VOPcPhO layer before the removal of the template is done. Once the templates are dissolved into NaOH, the formation of P3HT:VOPcPhO composite nanorods were observed (e).

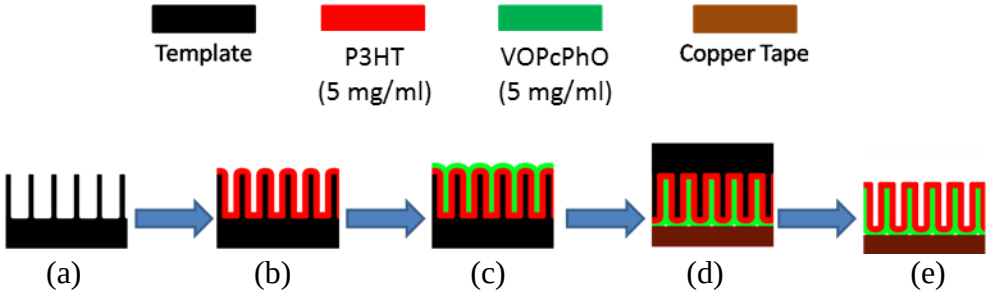

Figure 4.10: Schematic illustration of the formation process of P3HT:VOPcPhO composite nanorods

4.2 Optical Properties

The optical properties of VOPcPhO nanoflowers and P3HT:VOPcPhO composite nanorods are studied via Ultraviolet-Visible-Near Infrared (UV-VIS-NIR) Spectrophotometer and Raman spectroscopy.

4.2.1 UV-Vis Spectra

To determine the optical properties of VOPcPhO nanoflowers, ultraviolet-visible-near infrared (UV-Vis-NIR) absorption spectra have been carried out. Figure 4.11 (a) and (b) show the UV-vis absorption coefficient spectra of VOPcPhO nanostructures at 5 mg/ml and 15 mg/ml, respectively.

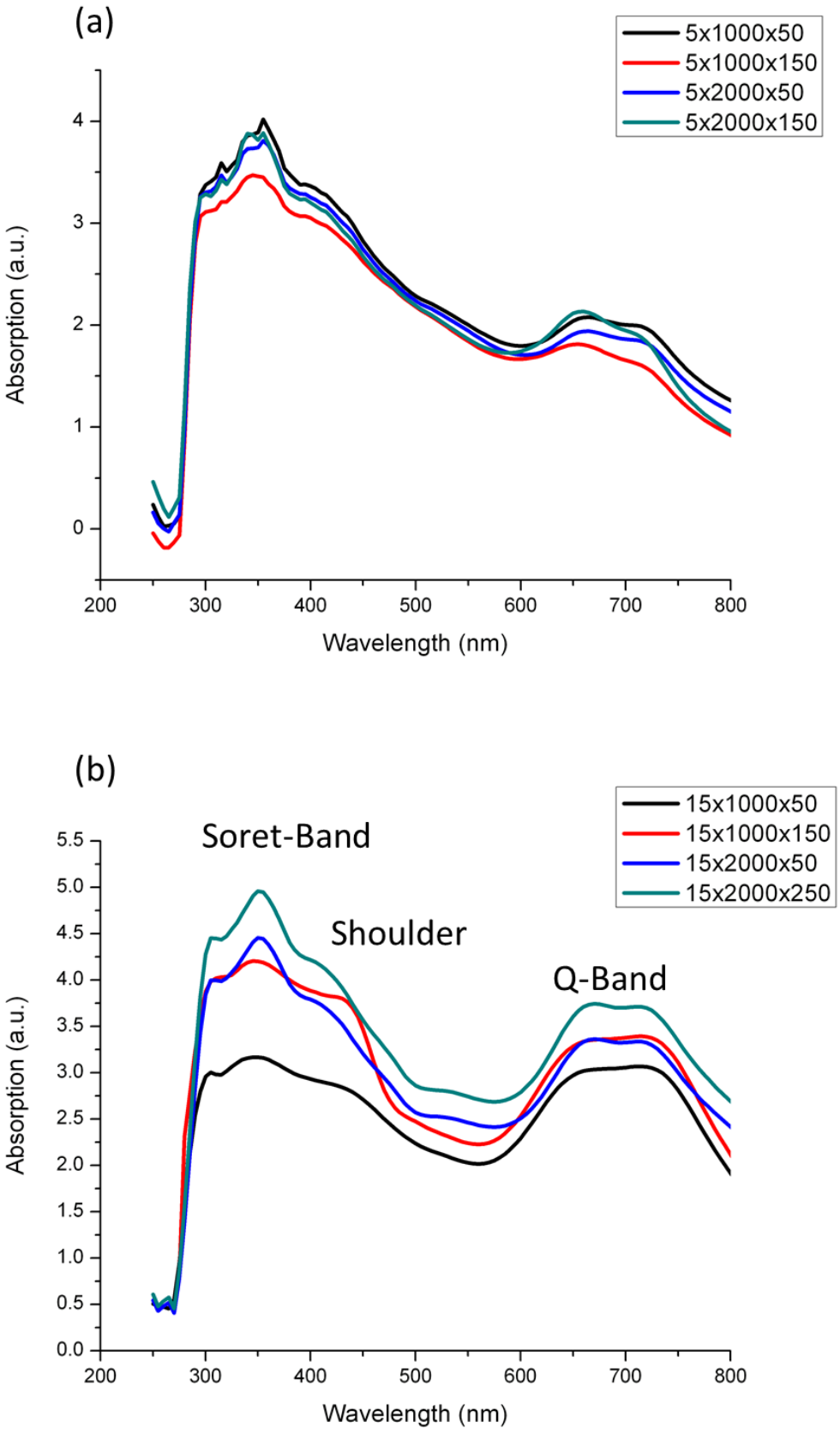

Figure 4.11: UV-vis spectra of VOPcPhO nanoflowers at (a) 5 mg/ml and (b) 15 mg/ml

From the UV-vis spectra, it is observed that VOPcPhO nanoflowers have two predominant bands in their absorption spectrum which is a Soret-Band and Q-Band. A well-known band in phthalocyanine molecules which is Q-band is observed to exist in the visible region between 630 nm to 750 nm while the Soret-band is observed in the UV region at a range of 270 nm to 410 nm [93]. The Soret-band consists of two peaks, Soret-band higher energy peak and Soret-band lowest energy peak and a shoulder at the higher wavelength. Q-band consists of two bands which is Q-band lowest energy peak and Q-band highest energy peak. In order to have a more details study on the UV-Vis spectra, total of eight samples of VOPcPhO thin films with a different in solution concentration, spin coating rate and annealing temperature were prepared and compared with the VOPcPhO nanostructures.

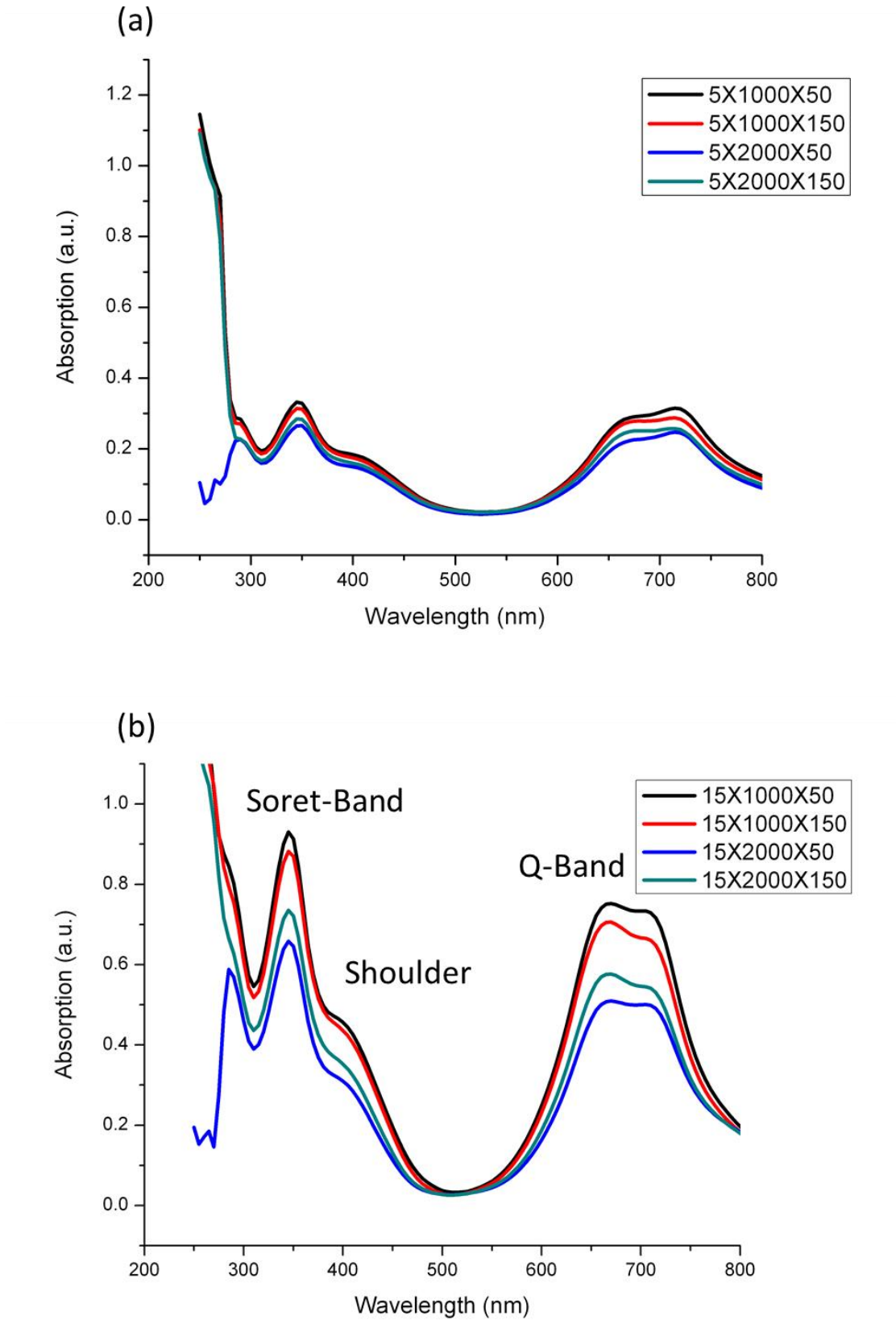

Figure 4.12: UV-vis spectra of VOPcPhO thin films at (a) 5 mg/ml and (b) 15 mg/ml

Figure 4.12 shows the UV-vis absorption coefficient spectra of VOPcPhO thin films at 5 mg/ml and 15 mg/ml. From Figure 4.12, it is observed that VOPcPhO thin films demonstrate two predominant bands same as for the VOPcPhO nanostructures. Having a closer look for both VOPcPhO thin films and nanostructures, it shows an upwards and downwards shift detected for certain peaks as shown in Figure 4.13. Difference in UV-vis spectrum between VOPcPhO thin films and nanostructures can be observed at the Q-band lowest energy peak. For VOPcPhO with concentration of 5 mg/ml, a blue shift to a shorter wavelength by 15 nm is observed. This indicated that the VOPcPhO nanostructures has a more dominant first π-π* transition on the phthalocyanine macrocycle. Even though the present of second π-π* transition is observed by VOPcPhO nanostructures, the improvement of second π-π* transition is exhibited by VOPcPhO thin films [93]. The Q-Band for VOPcPhO nanostructures for both 5 and 15 mg/ml are recorded to be wider compared to VOPcPhO thin films. This could be caused by the well-ordered structured of the tubular-shaped of VOPcPhO which explained the novel morphology of nanostructured materials.

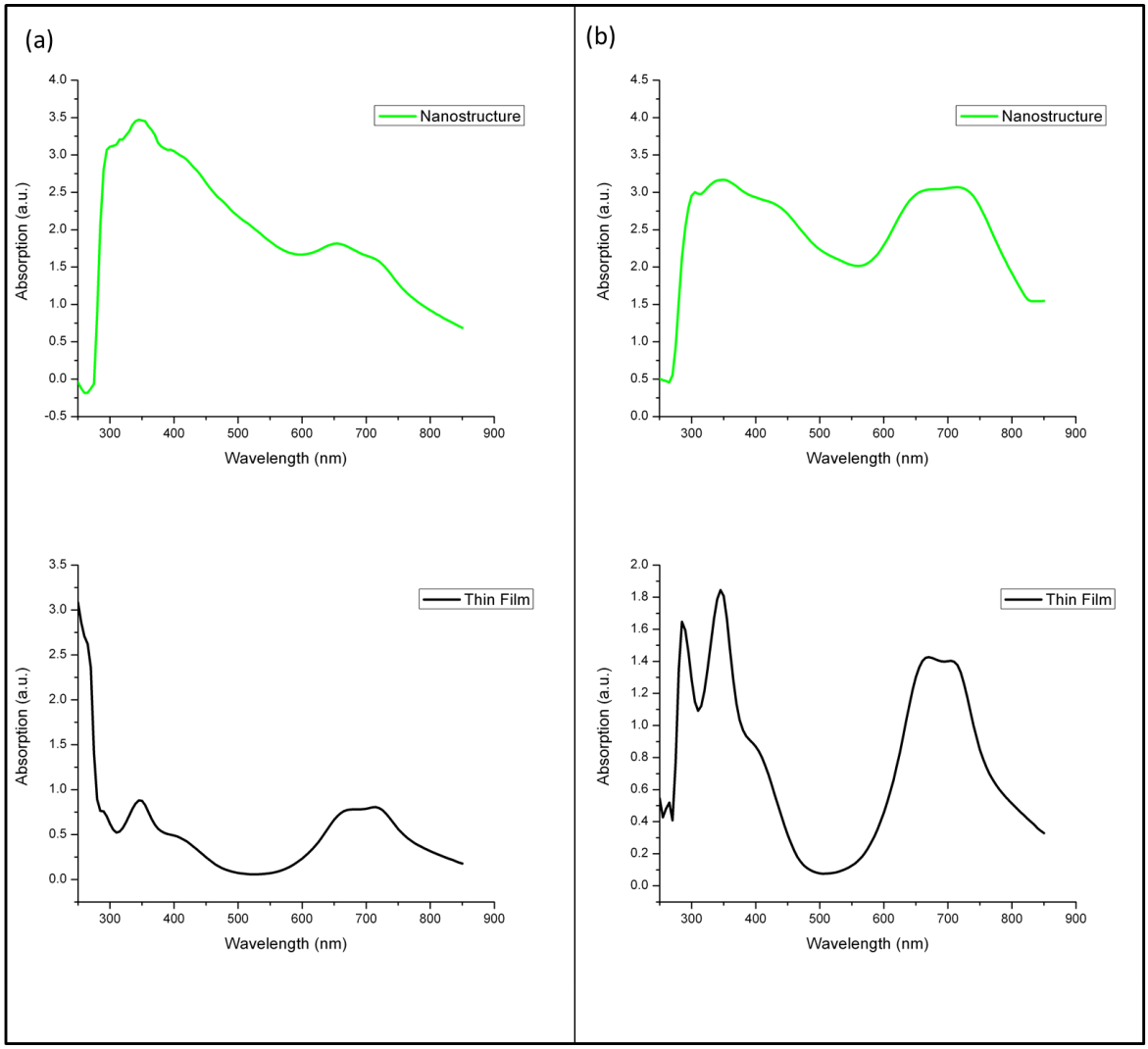

Figure 4.13: UV-vis spectra of VOPcPhO nanostructures and thin films at (a) 5 mg/ml and (b) 15 mg/ml

4.2.2 Raman Spectra

Raman spectra of VOPcPhO nanostructures at 5 mg/ml and 15 mg/ml are represented in Figure 4.14 (a) and (b), respectively. Figure 4.15 shows the Raman spectra of VOPcPhO thin films which employed as the reference to the VOPcPhO nanostructures.

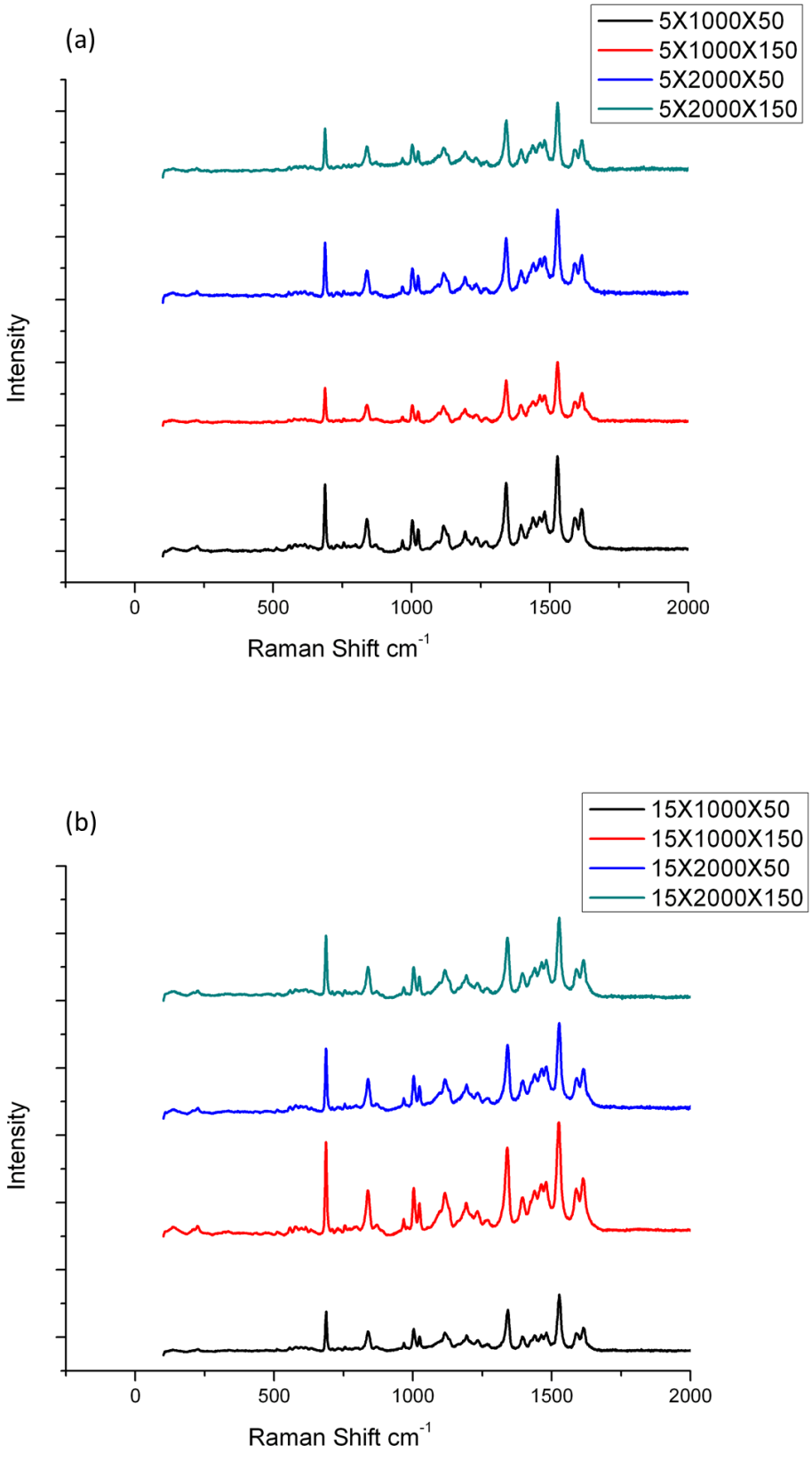

Figure 4.14: Raman spectra of VOPcPhO nanostructures at (a) 5 mg/ml and (b) 15 mg/ml

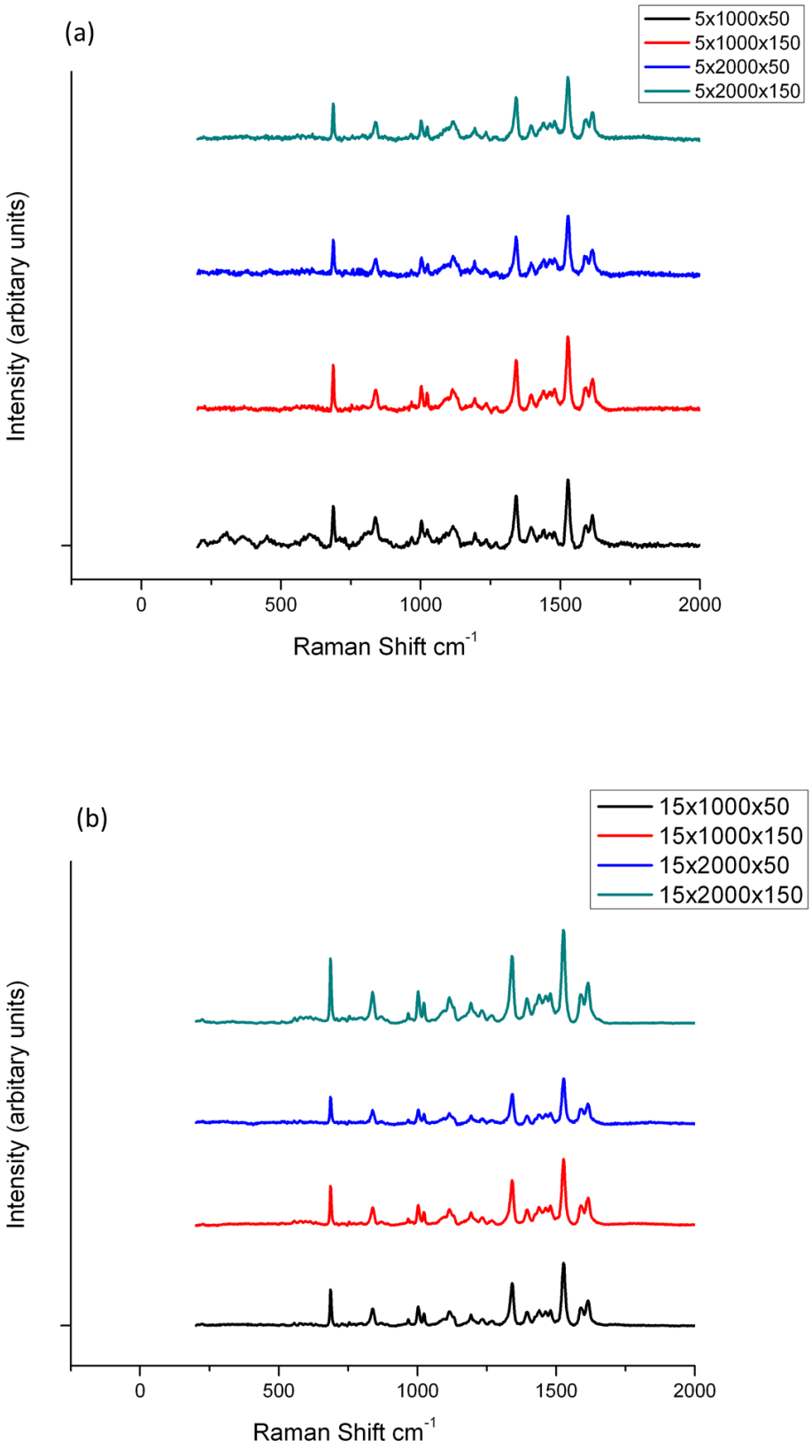

Figure 4.15: Raman spectra of VOPcPhO thin films at (a) 5 mg/ml and (b) 15 mg/ml

A difference in Raman spectra for VOPcPhO nanostructures and thin films is illustrated in Figure 4.16 (a) 5 mg/ml and (b) 15 mg/ml. There are several shift detected due to a certain assignments as tabulated in Table 4.2. Both VOPcPhO nanostructures and thin films have a peak due to VO stretch assignment which verified the materials as VOPcPhO. Red shift is observed from thin films to nanostructures by 1 nm in VO stretch assignment for 5 mg/ml but not for 15 mg/ml. The vibration associated with carbon-carbon stretching in benzene that is observed in the region of 1565 to 1620 cm^{-1} is very weak or absent [94]. A blue shift by 5 cm^{-1} at carbon-carbon stretching is detected for VOPcPhO nanostructures of 15 mg/ml. Other assignments including pyrole stretch, macrocyle stretching, benzene ring deformation and isoindole mostly recorded a red shift or no shift from thin films to nanostructures. For carbon-hydrogen bending and isoindole stretch, a minor blue shift can be observed.

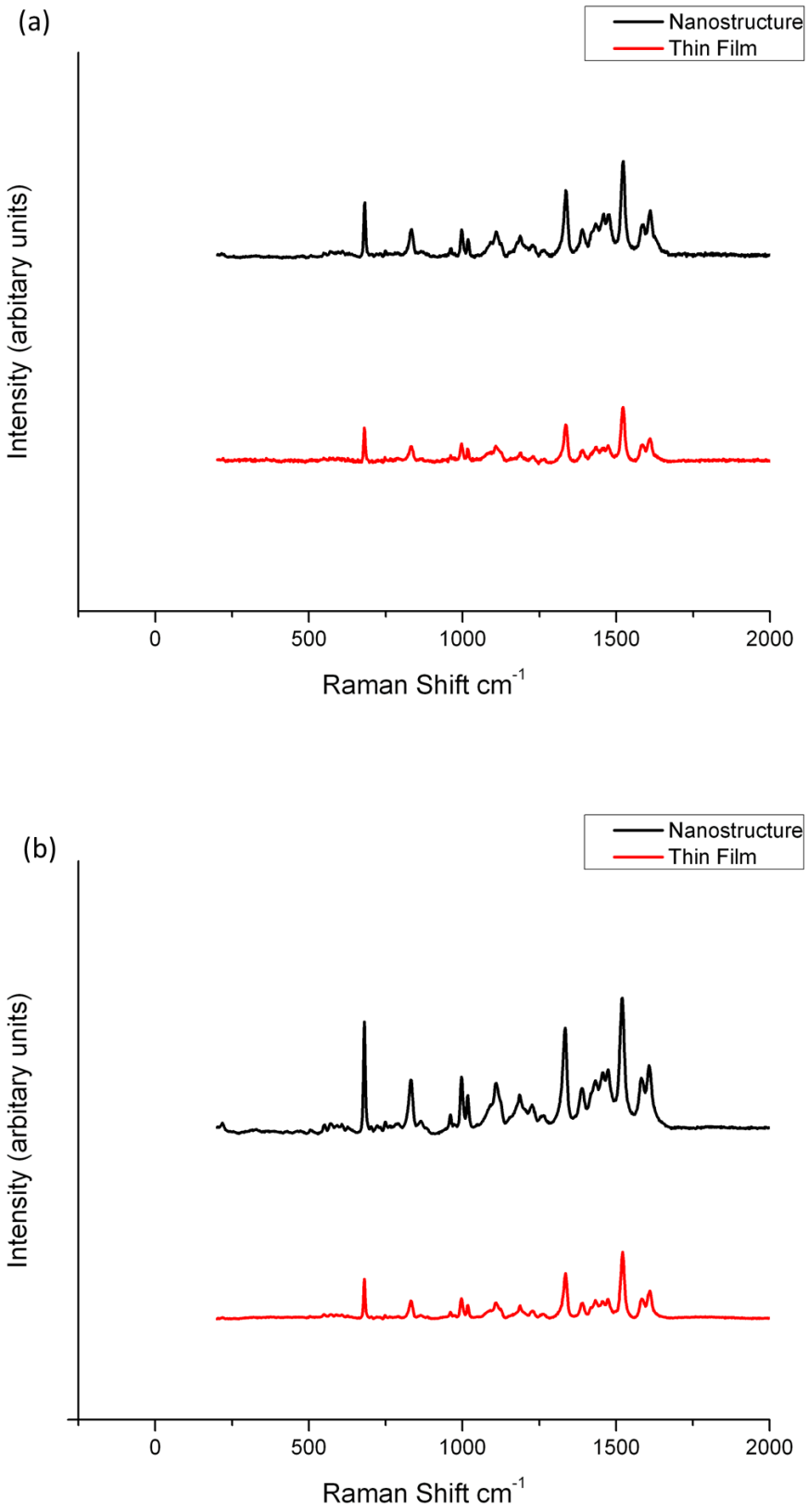

Figure 4.16: Raman spectra of VOPcPhO nanostructures and thin films at (a) 5 mg/ml and (b) 15 mg/ml

Figure 4.17 shows the Raman spectra of P3HT:VOPcPhO composite nanorods and thin films. Several absorption peak can be observed which corresponds to C-H stretching, C-C stretching, C=C stretching and C-H bending at 2897 cm^{-1}, 1520 cm^{-1}, 1449 cm^{-1}, 1380 cm^{-1}, 1003 cm^{-1} and 727 cm^{-1} [94]. The comparison between Raman spectra of P3HT:VOPcPhO composite nanorods and thin films show some minor shift in band wavenumbers. The changes of band wavenumbers between the nanostructures and thin films are tabulated in Table 4.3.

Table 4.2: Assignments associated to VOPcPhO Raman peak

Thin Film		Assignment	Nano-flower	
5/1000/150	15/1000/150		5/1000/150	15/1000/150
1615	1617	C=C stretch benzene	1615	1612
1527	1527	Pyrrole stretch	1528	1527
1478	1479	lsoindole stretch	1478	1479
1440	1437	lsoindole stretch	1395	1395
1341	1341	Pyrrole stretch	1341	1340
1234	1232	C-H bend	1234	1232
1195	1193	C-H bend	1193	1192
1113	1116	C-H bend	1115	1116
1003	1003	Benzene ring breathing	1003	1003
967	967	VO stretch	968	967
838	838	Macrocycle stretching	839	838
753	754	Macrocycle stretching	754	756
686	686	Macrocycle stretching	688	686
611	611	Benzene ring deformation	615	612
447	436	lsoindole ring deformation	482	

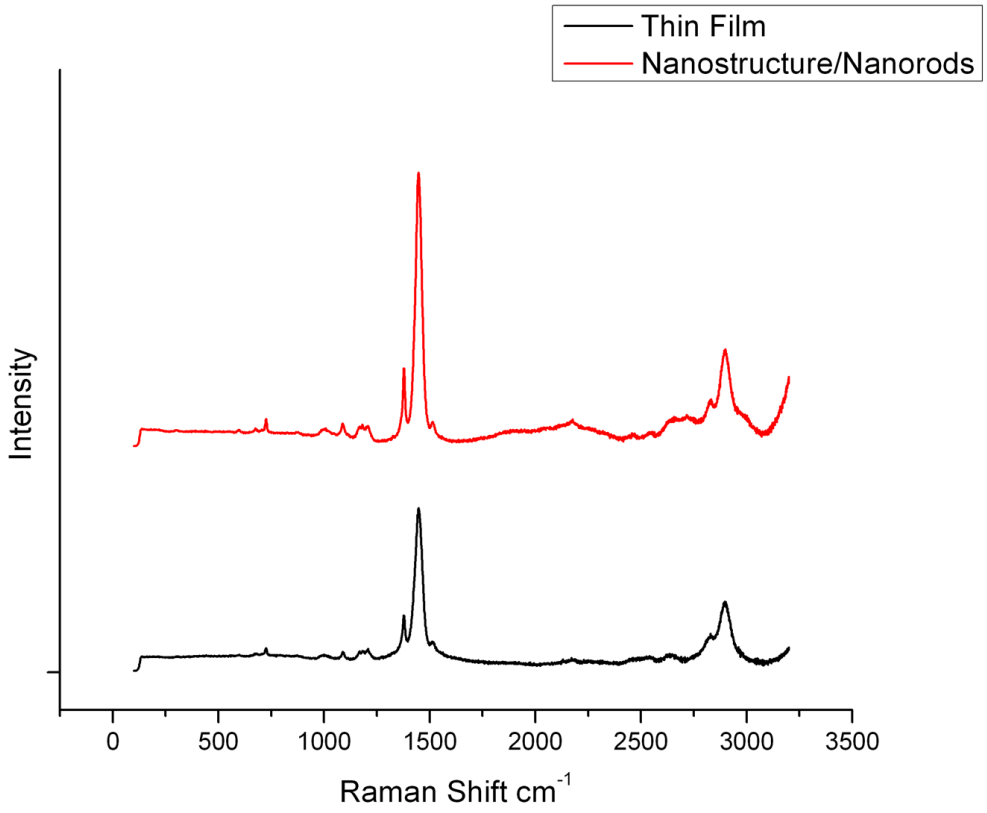

Figure 4.17: Raman spectra of P3HT:VOPcPhO composite nanorods and P3HT:VOPcPhO thin films

Table 4.3: Assignments associated to P3HT:VOPcPhO Raman peak

Thin Film	Assignment	Nano-flower
727	Macrocycle stretching	727
1003	Benzene ring breathing	1003
1091	C-H bending	1088
1182	C-H bending	1186
1201	C-H bending	1211
1380	C-C stretching	1380
1449	C=C stretching	1449
1520	Pyrole stretching	1520
2897	C-H stretching	2898
2897	C-H stretching	2897

CHAPTER 5

CONCLUSIONS

In conclusion, VOPcPhO nanoflowers and P3HT:VOPcPhO composite nanorods have been successfully synthesised by a simple solution process method via alumina porous template. The morphological, structural and optical properties of VOPcPhO and P3HT:VOPcPhO can be improved via the formation of nanoflowers and composite nanorods, respectively.

VOPcPhO nanoflowers consist of a group of rosette that form a structure of nanoflowers. FESEM and TEM images explained the formation of VOPcPhO nanoflowers. It can be postulated that the solution concentration, spin coating rate and annealing temperature has controlled the formation of VOPcPhO nanoflowers. Solution concentration has much effect on the infiltration rate. The better infiltration could be achieved by the higher solution concentration of 15 mg/ml. VOPcPhO nanoflowers shows a very intense absorption in UV-vis compared to its counterpart VOPcPhO thin films. The existence of nanoflowers and well-ordered nano tubular-shaped improve the optical properties of VOPcPhO. The optical properties of P3HT:VOPcPhO composite can also be enhanced by means of nanorods structure.

REFERENCES

1. S. Senthilkumaar, K. Rajendran, S. Banerjee, T. K. Chini, V. Sengodan. (2008). Influence of Mn doping on the microstructure and optical property of ZnO. *Materials Science Semiconductor Process*, 6-12.

2. M. M. Khalaf, H.G Ibrahimov, E. H Ismailov. (2012). Nanostructured Materials: Importance, Synthesis and Characterization - A Review. *Chemistry Journal*, 118-125.

3. C. S. Li, L. H. Jin, Z. M. Yu, S. N. Zhang, Y. F. Lu, J. Q. Feng. (2014). Enhanced flux pinning in YGdBCO film grown by sol–gel approach. *Journal of Sol-Gel Science and Technology*.

4. C. Jin, J. Wang, Y. Wang, H. Tang, T. Lu. (2014). Fabrication of hierarchically porous silica nanospheres through sol–gel process and pseudomorphic transformation. *Journal of Sol-Gel Science and Technology*.

5. S. P. Ashby, J. A. Thomas, P. R. Coxon, M. Bilton, R. Brydson, T. J. Pennycook, Y. Chao. (2013). The effect of alkyl chain length on the level of capping of silicon nanoparticles produced by a one-pot synthesis route based on the chemical reduction of micelle. *Journal of Nanoparticle Research, 15*(1425).

6. N. V. Sastry, A. D. Thummar, S. H. Punjabi. (2013). Mixed Micelles of Trisiloxane Based Silicone and Hydrocarbon Surfactants Systems in Aqueous Media: Dilute Aqueous Solution Phase Diagrams, Surface Tension Isotherms, Dilute Solution Viscosities, Critical Micelle Concentrations and Application of Regular S. *Journal of Surfactants and Detergents, 16*(6), 829-840.

7. P. E. Meskin, A. I. Gavrilov, V. D. Maksimov, V. K. Ivanov, B. P. Churagulov. (2007). Hydrothermal/microwave and hydrothermal/ultrasonic synthesis of nanocrystalline titania, zirconia, and hafnia. *Russian Journal of Inorganic Chemistry, 52*(11), 1648-1656.

8. J. P. G. Farr, A. J. S. McNeil. (1975). A study of the morphology of nickel electrodeposits and the influence of substrate and electrolyte, using high resolution replication. *Electrodeposition and Surface Treatment, 3*(5-6), 399–415.

9. Nageswar, S. (1975). Electrodeposition of copper on a copper single crystal (111) face in the presence of chloride ions. *Electrodeposition and Surface Treatment, 3*(5-6), 357–367.

10. H. Wang, X. Cao, J. Xu, C. Yuan, X. Zhang. (2012). Low temperature synthesis and properties of MgxZn1-x O:Al UV transparent conducting films by ultrasonic spray pyrolysis. *Journal of Materials Science: Materials in Electronics, 23*(7), 1327-1331.

11. X. Wang, H. Zhang, J. Li, L. Miao, Y. Yang. (2013). Effect of Eu doping concentration on the morphologies and optical properties of ZnO film prepared by ultrasonic spray pyrolysis. *Journal of Materials Science: Materials in Electronics, 24*(6), 1883-1887.

12. X. Wang, H. Zhang, J. Li, L. Miao, Y. Yang. (2013). Effect of Eu doping concentration on the morphologies and optical properties of ZnO film prepared by

ultrasonic spray pyrolysis. *Journal of Materials Science: Materials in Electronics, 24*(6), 1883-1887.

13. B. Kaur, H. Kumar. (2013). Methyltrioctylammonium chloride catalysed sonochemical synthesis of acridine diones. *Journal of Chemical Sciences, 125*(5), 989-992.

14. L. B. Arruda, D. M. G. Leite, M. O. Orlandi, W. A. Ortiz, P. Noronha Lisboa-Filho. (2013). Sonochemical Synthesis and Magnetism in Co-doped ZnO Nanoparticles. *Journal of Superconductivity and Novel Magnetism, 26*(7), 2515-2519.

15. L. X. Zhang, Y. X. Sun, H. F. Jiu, Y. H. Fu, Y. Z. Wang, J. Y. Zhang. (2012). Solvothermal synthesis of hollow Eu2O3 microspheres using carbon template-assisted method. *Chemical Papers, 66*(8), 741-747.

16. T. Wumair, J. Dou, L. Zhang, M. Chen, X. Kang. (2013). Synthesis of carbon microtubules core structure LiFePO4 via a template-assisted method. *Ionics, 19*(12), 1855-1860.

17. S. Honda, S. Yokoya, H. Ohkita, H. Benten, S. Ito. (2011). Light-harvesting mechanism in polymer/fullerene/dye ternary blends studied by transient absorption spectroscopy. *The Journal of Physical Chemistry C.*

18. L. Shen, G. Zhu, W. Guo, C. Tao, X. Zhang, C. Liu, W. Chen, S. Ruan, Z. Zhong. (2008). Performance improvement of TiO2/P3HT solar cells using CuPc as a sensitizer. *Applied Physics Letters*, 073307– 073309.

19. M. El-Nahass, K. Abd-El-Rahman, A. Darwish. (2005). Fourier-transform infrared and UV–Vis spectroscopes of nickel phthalocyanine thin films. *Materials Chemistry and Physics*, 1631–1636.

20. M. El-Nahass, S. Yaghmour. (2008). Effect of annealing temperature on the optical properties of thermally evaporated tin phthalocyanine thin films. *Applied Surface Science*, 1631–1636.

21. A. Kamarundzaman, M. S. Fakir, A. Supangat, K. Sulaiman, H. Zulfiqar. (2013). Morphological and optical properties of hierarchical tubular VOPcPhO nanoflowers. *Materials Letters*, 13-16.

22. Supangat, A. Kamarundzaman, N. A. Bakar, K. Sulaiman, H. Zulfiqar. (2014). P3HT:VOPcPhO composite nanorods arrays fabricated via template–assisted method:Enhancement on the structural and optical properties. *Materials Letters*, 103–106.

23. J. Moreira, N. Ordonez, R. D. Mansan. (2013). Low Pressure Plasma Study for Platinum Nanoparticles Synthesis. *Nanomaterials and nanotechnology, 3*.

24. P. Hazra, S. Jit. (2014). Electrical Characteristics of Si/ZnO Core–Shell Nanowire Heterojunction Diode. *Environmental Science and Engineering*, 673-675.

25. J. Deneen Nowak, Z. W. Shan, O. L. Warren. (2008). In situ characterization of the mechanical properties of nanoparticles and nanoscale structures. *EMC 2008 14th European Microscopy Congress 1–5 September 2008, Aachen, Germany*, 503-504.

26. J. Grunes, J. Zhu, G.A. Somorjai. (2003). *Catalysis 25 and Nanoscience. Chem. Comm* , 2257-2260.

27. Bell, A. (2003). The Impact of Nanoscience on Heterogeneous Catalysis. *Science*, 1688-1691.

28. N. Kaur, S. Gupta, K. Dharamvir, V.K. Jindal. (2009). Behaviour of a bucky-ball under extreme internal and external pressures. *Shock Waves*, 1017-1022.

29. S. Kumar, I. Kaur, N. Kumari, S. Jain, K. Dharamveer, V. K. Jindal, N. K. Verma, L. M. Bharadwaj. (2014). Atomic force microscope manipulation of multiwalled and single walled carbon nanotubes with reflux and ultrasonic treatments. *Applied Nanoscience, 4*(1), 19-26.

30. S. Kuchibhatla, A.S. Karakoti, D. Bera, S. Seal. (n.d.). *Prog. Mater. Sci*, 2007.

31. J. Weber, R. Singhal, S. Zekri, A. Kumar. (2008). *Inter. Mater. Rev.*

32. N. Wang, Y. Cai, R. Q. Zhang. (2008). *Mater. Sci. Eng. R.*

33. R. Rahimi, S. Kuchibhatla, D. Korakakis1. (2013). Effect of dielectric/organic interface properties on charge transport in organic thin film transistors. *Journal of Applied Physics, 113*(154305).

34. M. Moradi, M. Zamanian, M. Noormohammadi. (2013). Fabrication of various electrical resistances producing Zn nanowires and subsequent oxidation fabricating ZnO nanowires in PAA template by periodic and pulsed electrochemical deposition. *Journal of Nanostructure in Chemistry, 3*(6).

35. Z. Wei, Z. X. Feng, L. X. Ze, J. N. Er. (2010). Electrodeposition of mesoporous manganese dioxide nanowires arrays from a novel conjunct template method. *Journal of Porous Materials, 17*(2), 253-257.

36. Kumar, S. (2013). Structural, dielectric and magnetic characterization of large scale template synthesized Gd doped BiFeO3 nanowires. *Journal of Materials Science: Materials in Electronics, 24*(6), 2112-2115.

37. M. Norek, G. Luka, M. Godlewski, T. Plocinski, M. Michalska-Domanska, W. J. Stepniowski. (2013). Plasmonic enhancement of blue emission from ZnO nanorods grown on the anodic aluminum oxide (AAO) template. *Applied Physics A, 111*(1), 265-271.

38. Huang, L. Chen, G. Xu, L. Miao. (2012). Sol–gel template synthesis and characterization of VO2 nanotube arrays. *Journal of Sol-Gel Science and Technology*, 103-107.

39. H. Zhang, X. Zhang, T. Wu, Z. Zhang, J. Zheng, H. Sun. (2013). Template-based synthesis and discontinuous hysteresis loops of cobalt nanotube arrays. *Journal of Materials Science, 48*(21), 7392-7398.

40. Steinhart, M. (2008). Supramolecular Organization of Polymeric Materials in Nanoporous Hard Templates. *Advances in Polymer Science , 220*, 123-187.

41. J. P. Lee, S. Choi, S. Park. (2012). Preparation of silica nanospheres and porous polymer membranes with controlled morphologies via nanophase separation. *Nanoscale Research Letters, 7*(440).

42. N. Tasaltin, S. Öztürk, N. Kilinç, H. Yüzer, Z. Z. Öztürk. (2010). Fabrication of vertically aligned Pd nanowire array in AAO template by electrodeposition using neutral electrolyte. *Nanoscale Research Letters, 10*(1007).

43. W. Jessica, S. Rahul, Z. Souhail, K. Ashok. (2008). One-dimensional nanostructures: fabrication, characterisation and applications. *53*(4), 235-255.

44. G. She, L. Mu, W. Shi. (2009). Electrodeposition of One-Dimensional Nanostructures. 182-191.

45. L. Zaraska, G. D. Sulka, M. Jaskula. (2011). Anodic alumina membranes with defined pore diameters and thicknesses obtained by adjusting the anodizing duration and pore opening/widening time. *Journal of Solid State Electrochemistry, 11*(1471).

46. A. Ispas, A. Bund, I. Vrublevsky. (2010). Investigations on current transients in porous alumina films during re-anodizing using the electrochemical quartz crystal microbalance. *Journal of Solid State Electrochemistry, 14*(11), 2121-2128.

47. G. Patermarakis, G. Kapiris. (2013). Processes, parameters and mechanisms controlling the normal and abnormal growth of porous anodic alumina films. *Journal of Solid State Electrochemistry, 17*(4), 1133-1158.

48. G. Q. Ding, R. Yang, J. N. Ding, N. Y. Yuan, Y. Y. Zhu. (2010). Fabrication of Porous Anodic Alumina with Ultrasmall Nanopores. *Nanoscale Research Letters*.

49. H. L. Liraa, R. Patersonb. (2002). New and modified anodic alumina membranes : Part III. Preparation and characterisation by gas diffusion of 5 nm pore size anodic alumina membranes. *Journal of Membrane Science, 206*(1-2), 375–387.

50. M. Kokonou, K.P. Giannakopoulos, A.G. Nassiopoulou. (2007). *Journal of Membrane Science, 515*(7-8), 3602–3606.

51. G. Patermarakis, J. Chandrinos, K. Masavetas. (2007). Formulation of a holistic model for the kinetics of steady state growth of porous anodic alumina films. *Journal of Solid State Electrochemistry*, 1191-1204.

52. G. Patermarakis, K. Moussoutzanis, J. Chandrinos. (2001). Discovery by kinetic studies of the latent physicochemical processes and their mechanisms during the growth of porous anodic alumina films in sulfate electrolytes. *Journal of Solid State Electrochemistry*, 39-54.

53. M. Moradi, M. Zamanian, M. Noormohammadi. (2013). Fabrication of various electrical resistances producing Zn nanowires and subsequent oxidation fabricating ZnO nanowires in PAA template by periodic and pulsed electrochemical deposition. *Journal of Nanostructure in Chemistry*.

54. Y. T. Peng, Q. F. Chen. (2013). Fabrication and characterization of crystalline copper nanowires by electrochemical deposition inside anodic alumina template. *Chinese Science Bulletin*, 3409-3414.

55. L. A. S. de Oliveira, K. R. Pirota. (2012). Sol–gel route to prepare well-ordered nanowires with anodic aluminum oxide template. *Journal of Sol-Gel Science and Technology*, 275-278.

56. Huang, L. Chen, G. Xu, L. Miao. (2012). Sol–gel template synthesis and characterization of VO2 nanotube arrays. *Journal of Sol-Gel Science and Technology, 63*(1), 103-107.

57. Z. Liu, Z. Jin, W. Li, X. Liu. (2006). Ordered porous ZnO thin films formed by dip-coating method using PS templates. *Journal of Sol-Gel Science and Technology*, 25-30.

58. F. Márquez, C. Morant, V. López, F. Zamora, T. Campo, E. Elizalde. (2011). An alternative route for the synthesis of silicon nanowires via porous anodic alumina masks. *Nanoscale Research Letters*.

59. H. Masuda, K. Fukuda. (1995). Ordered metal nanohole arrays made by a two-step replication of honeycomb structures of anodic alumina. *Science* , 1466–1468.

60. V. M. Prida, J. García, L. Iglesias, V. Vega, D. Görlitz, K. Nielsch, E. Díaz, B. Castro, R. M. Reséndez, A. Ponce, C. Luna . (2013). Electroplating and magnetostructural characterization of multisegmented Co54Ni46/Co85Ni15 nanowires from single electrochemical. *Nanoscale Research Letters*.

61. P. X. Hou, C. Liu, C. Shi, H. M. Cheng. (2012). Carbon nanotubes prepared by anodic aluminum oxide template method. *Chinese Science Bulletin*, 187-204.

62. W. Y. Zhou, X. X. Zhang, D. Zhao, M. Gao, S. Xie. (2013). ZnO nanorods: morphology control, optical properties, and nanodevice applications. *Science China Physics, Mechanics and Astronomy*, 2243-2265.

63. Y. Djaoued, S. Balaji, N. Beaudoin. (2013). Sol–gel synthesis of mesoporous WO3–TiO2 composite thin films for photochromic devices. *Journal of Sol-Gel Science and Technology*, 374-383.

64. H. Kim, C. H. Jeon, Y. S. Lee, J. K. Han, Y. C. Choi, S. D. Bu. (2013). Photoluminescence of ultra-thin-walled Pb(Zr,Ti)O3 nanotubes synthesized in the porous alumina membrane template-directed method. *Journal of the Korean Physical Society*, 1040-1044.

65. Piwonski, A. Kisielewska, J. Marczak. (2013). The application of Langmuir–Blodgett technique in preparation of the macroporous titania coatings. *Journal of Porous Materials*, 1395-1404.

66. L. Qu, L, G. Shi, X. Wu, B. Fan. (2004). Facile Route to Silver Nanotubes. *Advanced Materials*, 1200–1203.

67. M. Zhou, M. Aryal, K. Mielczarek, A. Zakhidov, W. Hu. (2010). Hole mobility enhancement by chain allignment in nanoimprinted poly(3-hexylthiophene)nanograting for organic electronic.

68. Roncali, J. (2007). Molecular Engineering of the Band Gap of p-Conjugated Systems: Facing Technological Applications. *Macromol. Rapid Commun*, 1761–1775.

69. Dodabalapur, A. (2006). Organic and polymer transistors for electronics. *Materials Today*, 24–30.

70. G. B. Street, T. C. Clark. (1981). Conducting Polymer:A review of recent work. *IBM Journal of Research and Development*, 51-57.

71. Roncali, J. (1992). Conjugated poly(thiophenes): synthesis, functionalization and applications. *Chemical Review*.

72. Roncali, J. (1997). Synthetic Principles for Bandgap Control in Linear π-Conjugated Systems. *Chemical Reviews*, 173–206.

73. Sellam, S. A. Hashmi. (2013). Quasi-solid-state pseudocapacitors using proton-conducting gel polymer electrolyte and poly(3-methyl thiophene)–ruthenium oxide composite electrodes. *Journal of Solid State Electrochemistry*.

74. Kareiyama, H. Nalwa H. (1997). *Handbook of Conductive 31 Molecules and Polymers.* New York: Wiley.

75. S. Kelkar, A. B. Chourasia. (2012). Effect of dopant on thermal properties of polythiophene. *Indian Journal of Physics*, 101-107.

76. S. M. Abdullah, Z. Ahmad, F. Aziz, K. Sulaiman. (2012). Investigation of VOcPhO as an acceptor meterial for bulk heterojunction solar cell. *Organic Electronic*, 2532-2537.

77. G. Schopf, G. Koβmehl. (1997). Polythiophenes-electrically conductive polymers. 3-145.

78. M. Zhou, M. Aryal, K. Mielczarek, A. Zakhidov, W. Hu. (2010). Hole mobility enhancement by chain allignment in nanoimprinted poly(3-hexylthiophene)nanograting for organic electronic.

79. A.M. Ballantyne, L. Chen, J. Dane, T. Hammant, F.M. Braun, M. Heeney et al. (2008). The effect of poly(3-hexylthiophene molecular weight on charge transport and the performance of polymer:fullerene solar cells. *Advance Functional Materials*, 2373-2380.

80. Bundgaard, F. C. Krebs. (2007). Low band gap polymer for organic photovoltaics. *Solar Energy Materials and Solar Cell*, 954-985.

81. T. A. Skotheim, R. L. (1998). *Handbook of Conducting Polymers.* M. Dekker.

82. N. N. Greenwood, A. Earnshaw. (1997). *Chemistry of the Elements. 2nd Eddition.* Elsevier.

83. G. Chaidogiannos, F. Petraki, N. Glezos, S. Kennou, S. Nešpurek. (2009). Low voltage operating OFETs based on solution-processed metal phthalocyanines. Applied Physics A: Materials Science and Processing, 763-767.

84. S. Honda, S. Yokoya, H. Ohkita, H. Benten, S. Ito. (2011). Light-harvesting mechanism in polymer/fullerene/dye ternary blends studied by transient absorption spectroscopy. *The Journal of Physical Chemistry C.*

85. L. Shen, G. Zhu, W. Guo, C. Tao, X. Zhang, C. Liu, W. Chen, S. Ruan, Z. Zhong. (2008). Performance improvement of TiO2/P3HT solar cells using CuPc as a sensitizer. *Applied Physics Letters*, 073307– 073309.

86. M. El-Nahass, K. Abd-El-Rahman, A. Darwish. (2005). Fourier-transform infrared and UV–Vis spectroscopes of nickel phthalocyanine thin films. *Materials Chemistry and Physics*, 1631–1636.

87. M. El-Nahass, S. Yaghmour. (2008). Effect of annealing temperature on the optical properties of thermally evaporated tin phthalocyanine thin films. *Applied Surface Science*, 1631–1636.

88. S. M. Khan, M. H. Sayyad, K. S. Karimov. (2011). Investigation of temperature dependent electrical properties of p-VOPc/n-si heterojunction under dark conditions. *Ionics*, 307–313.

89. R. O. Al-Kaysi, T. K. Ghaddar, G. Guirado. (2009). Fabrication of one dimensional organic nanostructures using anodic aluminum oxide templates. *Journal of Nanomaterials*, 1–14.

90. Amelinckx, S. (1997). *Handbook of Microscopy. Applications.* VCH.

91. Vandenabeele, P. (2010). Raman spectroscopy. *Analytical and Bioanalytical Chemistry*.

92. Mulder, M. (1996). *Basic Principles of Membrane Technology*. Kluwer Academic Publisher.

93. Aziz, M. H Sayyad, Z. Ahmad, K. Sulaiman, M. R. Muhammad, Kh. S. Karimov. (2012). Spectroscopic and microscopic studies of thermally treated Vanadyl 2,9,16,23-tetraphenoxy-29H,31H-phthalocyanine thin films. *Physica E*, 1815-1819.

94. C.A. Jeannings, R. Aroca, G. J. Kovacs, C. Hsaio. (1996). FT-Raman Spectroscopy of Thin Films of Titanyl Phthalocyanine and Vanadyl Phthalocyanine. *Journal of Raman Spectroscopy*, 867-872.

Materials Letters 111 (2013) 13–16

Contents lists available at ScienceDirect

Materials Letters

journal homepage: www.elsevier.com/locate/matlet

Morphological and optical properties of hierarchical tubular VOPcPhO nanoflowers

Anas Kamarundzaman [a], Muhamad Saipul Fakir [a], Azzuliani Supangat [a,*], Khaulah Sulaiman [a], Hadi Zulfiqar [b]

[a] Department of Physics, Faculty of Science, University of Malaya, Kuala Lumpur 50603, Malaysia
[b] Newcastle Innovation Ltd., The University of Newcastle, Callaghan, NSW 2308, Australia

ARTICLE INFO

Article history:
Received 24 June 2013
Accepted 15 August 2013
Available online 23 August 2013

Keywords:
Microstructure
Structural
Nanoflower
Template
Optical materials and properties

ABSTRACT

In this study, the morphological and optical properties of hierarchical tubular vanadyl 2,9,16,23-tetraphenoxy-29H,31H-phthalocyanine (VOPcPhO) flower-like nanostructures were reported. VOPcPhO nanoflowers have been synthesised from the solution concentration of 5 mg/ml via the template-assisted method. Dissolution of template has led to the growth of micrometer-sized flowers that have nanoscale features that are tubular shaped with protruding tips. The tubulars are self-assembled during the formation of flower-like nanostructures. UV–vis spectrum of VOPcPhO nanoflower shows a wider absorption at Q-band as compared to thin film. The changes in Raman shift were also observed which indicate the improvement of nanostructures exhibited by VOPcPhO nanoflowers.

1. Introduction

The studies on the morphological and optical properties of organometallic nanostructured compounds such as metal phthalocyanines (MPcs) are vital for the elaboration of electronic devices. Vanadyl 2,9,16,23-tetraphenoxy-29H,31H-phthalocyanine (VOPcPhO) is a dye pigment that consists of a central metallic (vanadium) atom bound to a π-conjugated ligand. It is one of the prominent MPcs which is well-known for its noteworthy properties such as high thermal stabilities [1], semiconductivity [2,3] and photoconductivity [4].

Nanostructured MPcs TNFePc nanoflowers, CuPc nanoflowers and nanoribbons, NiPc nanoribbons, CoPc nanowires and ZnPc nanoribbons have been widely reported for their application in various fields [5–7]. Novel nanostructured nanoflower has stimulated a great deal of interest which is potentially used in a field emitter, capacitor, gas sensor and battery [5,8–11]. The synthesis of nanoflower can be done via vapour-phase deposition, solvothermal, photochemical and hydrothermal methods, with or without the assistance of template [5–8,10,12]. Currently, a big challenge is to develop a simple and useful growth synthesis for the facile preparation of nanoflowers.

In this paper, we report the superficial solution synthesis of unique VOPcPhO nanoflowers assembled from the tube-like nanostructure with protruding tips. The synthesis is fully assisted by a porous alumina template. Based on the studies, the morphological and optical properties of VOPcPhO nanoflower are discussed in details.

2. Experimental

The commercially available VOPcPhO from Sigma-Aldrich was used without further purification. 5 mg/ml solution of VOPcPhO in chloroform was prepared. The porous alumina templates used in this study were commercially available filter membrane (Whatman Anodisc) with nominal pore diameters of 20 nm and a thickness of 60 μm. The templates were cleaned prior to use by sonicating in water and acetone for 10 min. Drop casting and spin coating technique were performed in order to obtain the nanostructures. 5 mg/ml of VOPcPhO was dropped onto the cleaned porous alumina template prior to the spin coating process at 1000 rpm. Then, the spin-coated VOPcPhO nanostructures within the alumina template were annealed at 150 °C. After annealing process, the alumina template was dissolved in 3 M NaOH and the remaining VOPcPhO nanostructures were rinsed in deionized water prior to its characterisation. The VOPcPhO nanoflowers were characterised by Field Emission Scanning Electron Microscopy (FESEM-EDX) (Quanta FEG 450), Transmission Electron Microscopy (TEM) (Tecnai G2 FEI), UV–vis spectroscopy (Shimadzu UV-3101PC), Raman spectroscopy (RENISHAW) and X-ray Diffraction spectroscopy.

* Corresponding author. Tel.: +60 192682768; fax: +60 379674146.
E-mail addresses: azzuliani@um.edu.my, azzuliani@yahoo.com (A. Supangat).

0167-577X/$ - see front matter © 2013 Elsevier B.V. All rights reserved.
http://dx.doi.org/10.1016/j.matlet.2013.08.064

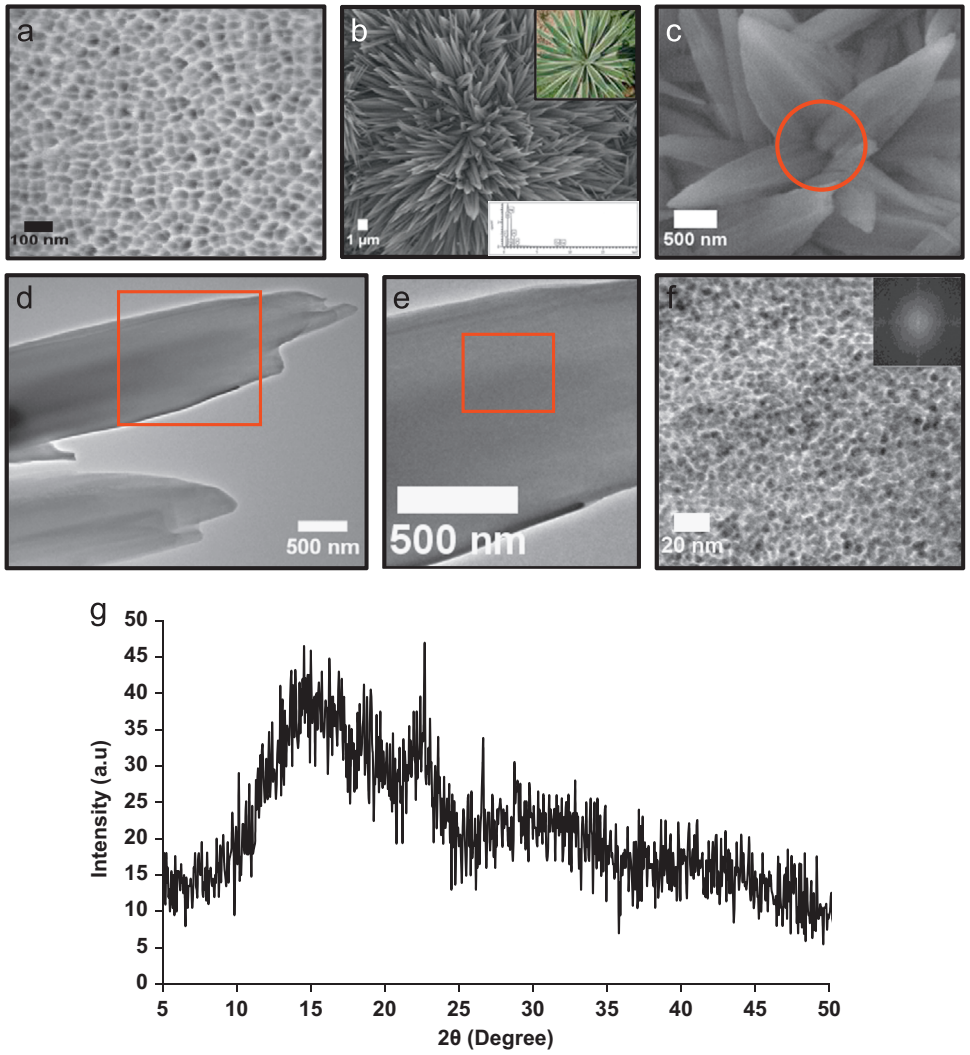

Fig. 1. (a) FESEM image of porous alumina template, (b) and (c) FESEM images of VOPcPhO nanoflowers (upper inset shows *Agave* and lower inset shows EDX spectrum), (d)–(f) TEM images of VOPcPhO nanoflowers (inset shows the FFT) and (g) XRD spectrum of VOPcPhO nanoflower. (For interpretation of the references to colour in this figure, the reader is referred to the web version of this article.)

3. Results and discussion

FESEM image of cleaned porous alumina template without any deposition of solution is shown in Fig. 1(a). The nominal template pore diameter is 20 nm and exhibits a hexagonal honeycomb network. The densely well-distributed hierarchical tubular VOPcPhO flower-like nanostructure is observed after the dissolution of template (Fig. 1(b)). VOPcPhO nanoflowers consist of a rosette which is long, spear-shaped and propagated. The rosette form is the structure, the relationship of the parts, and the variations within it. Interestingly, the VOPcPhO nanoflowers have not replicated the structure of porous template especially its diameter. With respect to the hexagonal porous structure of template, the expected formations such as nanotubes or nanorods were likely to be formed. However, the tubular-shaped VOPcPhO is successfully obtained from the efficient infiltration process. As shown in Fig. 1(b) upper inset, the morphology of VOPcPhO nanoflowers is analogue to the plant named *Agave*. *Agave* is also known as a dandelion which is defined as a cluster of leaves in crowded circles or spirals arising basally from a crown. EDX spectrum of VOPcPhO nanoflower is shown in Fig. 1(b) lower inset. Carbon (C), oxygen (O), sodium (Na), aluminium (Al) and copper (Cu) have been traced from the nanoflowers. C and O are obtained from VOPcPhO, Na is from NaOH and both Al and Cu are from sample holder and tape, respectively. Fig. 1(c) shows that the tubular-shaped VOPcPhO begins to grow from its base and further pair up together to form gigantic flower-like hierarchical structures. The tubular-shaped VOPcPhO came together and formed the closely-packed nanoflowers with an average diameter of ~500 nm. It demonstrates that the template has provided a nucleation site for the assembling of tubular-shaped VOPcPhO. This therefore plays a crucial role in producing the unique flower-like nanostructures. VOPcPhO nanoflowers comprise of a radial arrangement of vertically spread tubular-shaped nanostructure which binds at the base (node). In addition, the array of VOPcPhO portrays a circular arrangement of tubular-shaped nanostructure with protruding tips that radiate out from a centre close to the node. Finally, the VOPcPhO nanoflowers with numerous tubular-like structures form via the oriented attachment process. Generally, each tubular is in a sharp point of smooth margin and spring from the node. VOPcPhO that has been drop-casted onto a template has undergone the wetting process between liquid (solution) and solid (template) surface. Spin coating at 1000 rpm and annealing temperature at 150 °C has enhanced the wetting process by improving the infiltration.

A TEM image of an individual tubular VOPcPhO is shown in Fig. 1(d). The tips of the spikes is protruded into an irregular morphology. The bottom part of tubular's wall shows a more regular morphology although being asymmetrical. The protruding tips have formed a flower-like morphology which has not previously been reported with the manipulation of the porous alumina template. Magnified view of the red box in Fig. 1(d) is illustrated in Fig. 1(e). TEM images of VOPcPhO nanoflower has shown spectacular tubular-shaped nanostructures with regular wall. Interestingly, the diameter of tubular (~500 nm) is 25 times bigger than the template nominal pore diameter of 20 nm. This phenomenon could be expected from the expansion during the template removal process. Fig. 1(f) presents the high-resolution TEM image of an individual tubular that has been magnified from the red box in Fig. 1(e).

It suggests that there is an arrangement of VOPcPhO molecules within the flower-like nanostructures. VOPcPhO molecule organises itself in hexagonal honeycomb network which represents the molecular aggregation. The inset in Fig. 1(f) shows the fast Fourier transform (FFT) of TEM image which confirms the amorphous structure of VOPcPhO. Visible domains revealed that VOPcPhO nanoflower consists of regular spherical nanoparticles with diameters ranging from 1 to 5 nm. The postulation on the formation of tubular-shaped VOPcPhO has been supported by the TEM images that are obtained in the present studies. The XRD spectrum in Fig. 1(g) shows that the VOPcPhO nanoflower is amorphous and not crystalline. The weak peaks are located at 14.9° and 22.7° which support the amorphous structure of VOPcPhO that has been previously conveyed by FFT of TEM image.

A schematic illustration of the proposed formation of VOPcPhO nanoflowers is presented in Fig. 2. The VOPcPhO has infiltrated into a template after the annealing process is applied at 150 °C (a). The protruding tips are observed to grow within the template's pores. Before the dissolution of template, VOPcPhO is attached to the copper tape which portrays the upside down formation (b). After the dissolution, VOPcPhO nanoflowers are formed by the self-assembly of numerous tubular-shaped nanostructures (c).

Fig. 3(a) shows the UV–vis absorption spectra of VOPcPhO nanoflower and VOPcPhO thin film. It is seen that both VOPcPhO nanoflower and thin film portray two predominant bands. These bands are assigned as Soret-band and Q-band which exist in the UV region between 300 and 410 nm and in the visible region between 630 and 750 nm, respectively [1]. The Soret-band exhibits a peak with a shoulder appearing at 385 nm. In the UV region, VOPcPhO nanoflower and VOPcPhO thin film exhibit similar peak absorption for Soret-band at 345 nm. A difference between VOPcPhO nanoflower and thin film spectrum has been observed at the first peak of Q-band of VOPcPhO nanoflower in which a perceptible shift to the shorter wavelength occurred by 25 nm. However, a wider Q-band absorption of VOPcPhO nanoflower is observed as compared to thin film. The wider Q-band could be due to the well-distributed hierarchical tubular-shape of VOPcPhO nanoflower which indicates the novel morphology of nanostructured materials. In addition, the absorption pattern of the Davydov splitting that occurred at Q-band has been much influenced by the relative orientation of molecules [1]. At the Q-band of VOPcPhO nanoflower and thin film, the stronger peaks occurred at 655 nm and 715 nm, respectively. This indicates that the first π–π^* transition on the phthalocyanine macrocycle is more dominant for the VOPcPhO nanoflower rather than VOPcPhO thin film. Although the presence of second π–π^* transition is observed by VOPcPhO nanoflower, the improvement of second π–π^* transition is exhibited by VOPcPhO thin film. Raman spectra of VOPcPhO nanoflower and thin film are shown in Fig. 3(b). Similar absorption peaks at 1615 cm^{-1}, 1341 cm^{-1}, 1234 cm^{-1} and 1003 cm^{-1} are observed for C=C stretch benzene, pyrrole stretch, C–H bend and

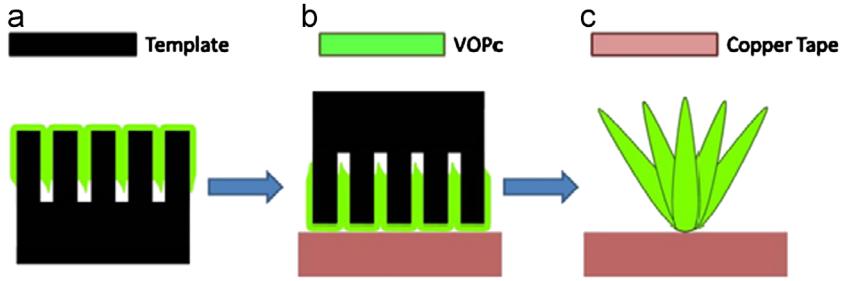

Fig. 2. Schematic illustration of the formation processes of VOPcPhO nanoflowers.

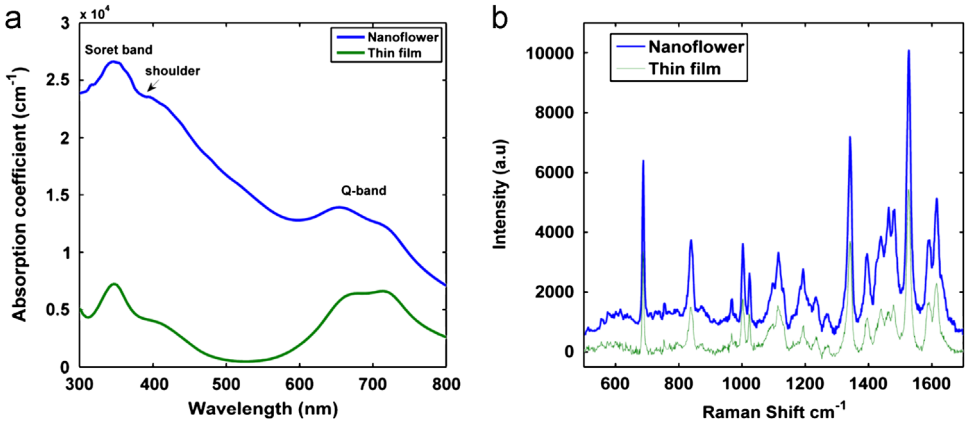

Fig. 3. (a) UV–vis absorption spectra and (b) Raman spectra of VOPcPhO nanoflower and thin film.

Table 1
Raman peak positions of VOPcPhO nanoflowers and thin film.

Raman shift (cm^{-1})		
Thin film	**Nanoflowers**	**Assignments**
687	688	Macrocycle breathing
838	840	Macrocycle stretching
967	968	VO stretch
1003	1003	Benzene ring breathing
1022	1025	C–H bend
1113	1115	C–H bend
1195	1193	C–H bend
1234	1234	C–H bend
1271	1272	C–H bend
1341	1341	Pyrrole stretch
1440	1439	Isoindole stretch
1465	1464	Isoindole stretch
1527	1528	Pyrrole stretch
1615	1615	C═C Stretch benzene

benzene ring breathing, respectively [13]. There are some minor shift in band wavenumbers and relative intensities between VOPcPhO nanoflowers and thin film. The changes of band wavenumbers between VOPcPhO nanoflowers and thin film are tabulated in Table 1. The Raman shift of C–H bending of nanoflowers is located at 1025 cm^{-1}, showing an apparent upward shift of about 3 cm^{-1}. This could be due to the better molecular arrangement of nanostructured materials exhibit by VOPcPhO nanoflowers [14].

4. Conclusions

In this work, VOPcPhO nanoflowers have been synthesised by a simple solution process method via porous alumina template. The morphological and optical properties of VOPcPhO can be improved via the formation of nanoflowers.

Acknowledgement

The authors would like to acknowledge University of Malaya and Ministry of Education Malaysia for project funding under Short Research Grant (BK026-2011A) and University of Malaya High Impact Research Grant UM-MOHE (UM.C/625/1/HIR/MOHE/SCI/26).

References

[1] Aziz F, Sayyad MH, Ahmad Z, Sulaiman K, Muhammad MR, Karimov KS. Physica E 2012;44:1815–9.
[2] Le PY, Dong LX, Juan WY, Bing CL, Yuan ZY, Hua SY, et al. Thin Solid Films 1998;324:209–13.
[3] Khan SM, Sayyad MH, Karimov KS. Ionics 2011;17:307–13.
[4] Abdullah SM, Ahmad Z, Aziz F, Sulaiman K. Organic Electronics 2012;13:2532–7.
[5] Mu J, Shao C, Guo Z, Zhang M, Zhang Z, Zhang P, et al. Nanoscale 2011;3:5126–31.
[6] Karan S, Basak D, Mallik B. Chemical Physics Letters 2007;434:265–70.
[7] Tong WY, Djurisic AB, Xie MH, Ng ACM, Cheung KY, Chan WK, et al. Journal of Physical Chemistry B 2006;110:17406–13.
[8] Li YB, Bando Y, Golberg D. Applied Physics Letters 2003;82:1962–4.
[9] Pavitra E, Yu JS. Materials Letters 2013;90:134–7.
[10] Wu M, Zeng W, Li Y. Materials Letters 2013.
[11] Yang Y, Jin R, Song S, Xing Y. Materials Letters 2012;93:5–8.
[12] Zhao WB, Zhu JJ, Xu JZ, Chen HY. Inorganic Chemistry Communications 2004;7:847–50.
[13] Jennings CA, Aroca R, Kovacs GJ, Hsaio CJ. Raman Spectroscopy 1996;27:867–72.
[14] Coppede N, Castriota M, Cazzanelli E, Forti S, Tarabella G, Toccoli T, et al. Journal of Physical Chemistry C 2010;114:7038–44.

Materials Letters 118 (2014) 103–106

Contents lists available at ScienceDirect

Materials Letters

journal homepage: www.elsevier.com/locate/matlet

P3HT:VOPcPhO composite nanorods arrays fabricated via template–assisted method: Enhancement on the structural and optical properties

Azzuliani Supangat [a,*], Anas Kamarundzaman [a], Nor Asmaliza Bakar [a], Khaulah Sulaiman [a], Hadi Zulfiqar [b]

[a] Low Dimensional Materials Research Centre, Faculty of Science, University of Malaya, Kuala Lumpur 50603, Malaysia
[b] Newcastle Innovation Ltd., The University of Newcastle, Callaghan, NSW 2308, Australia

ARTICLE INFO

Article history:
Received 4 November 2013
Accepted 11 December 2013
Available online 19 December 2013

Keywords:
Nanocomposite
Structural
Template
Optical materials and properties

ABSTRACT

In this study, the fabrication of poly(3-hexylthiophene-2,5-diyl) (P3HT) and vanadyl 2,9,16,23-tetraphenoxy-29H,31H phthalocyanine (VOPcPhO) composite nanorods is reported. P3HT:VOPcPhO composite nanorods have been synthesised from the solution concentration of 5 mg/ml via the template-assisted method. TEM images show that P3HT nanotube was first produced which has led to the infiltration of VOPcPhO. The composite nanorods have replicated the porous diameter of template of ~200 nm. If compared to the P3HT:VOPcPhO composite thin film, UV–vis spectrum of composite nanorods shows a wider band absorption and the peak absorption was shifted to the longer wavelength, which could be due to the improved interaction between small molecules and P3HT segment at their interfaces. The better absorption that portrayed by composite nanorods was supported by the quenching of intense peak in photoluminescence spectrum. Owing to the quenching, the photo-induced charge transfer and charge carrier dissociation in the composite nanorods is pragmatic.

1. Introduction

The studies on the fabrication of polymer and dye material composites are essential for the facile production of electronic devices. Conjugated polymer and dye material composites have attracted much research interest due to their potential for low cost electronic devices such as sensors, solar cells and capacitors [1–4]. The dielectric, mechanical, structural, optical and electrical properties of nanocomposites have been widely reported for their exceptional features [2,5–8]. Typically, the preparation of nanocomposites is performed via a blending/mixing solution method [1–4] which will only produce the composite thin films instead of novel nanostructured composite. The approach to the highly facile fabrication of novel nanostructured composite can be realised via the integration of templating method [6,9–11]. Polymer of poly (3 hexylthiophene 2,5 diyl) (P3HT) and dye material of vanadyl 2,9,16,23 tetraphenoxy 29H,31H phthalocyanine (VOPcPhO) composite thin films have been reported to have an enhancement on its optical properties [1]. In conjunction with this finding, a novel nanostructured composite composed of P3HT and VOPcPhO would potentially stimulate a great deal of interest in producing the remarkable electronic devices.

In this paper, we report the production of novel polymer/dye composite nanorods with enhanced structural and optical properties. The preparation of P3HT:VOPcPhO composite nanorods is fully assisted by a porous alumina template. Based on the studies, the comparison of structural and optical properties between P3HT:VOPcPhO composite nanorods and thin films are discussed in details.

2. Experimental

The P3HT and VOPcPhO from Sigma Aldrich were used without further purification. P3HT and VOPcPhO were dissolved in chloroform and prepared in the solution concentration of 5 mg/ml, respectively. The porous alumina templates used in this study were commercially available filter membrane (Whatman Anodisc) with nominal pore diameters of 200 nm and a thickness of 60 μm. 5 mg/ml of P3HT was first dropped onto the cleaned porous alumina template, spin coated at 1000 rpm and annealed at 150 °C prior to the drop casted of VOPcPhO of the same spin coating's speed. After annealing process, the alumina template was dissolved in 3 M sodium hydroxide and the remaining P3HT:VOPcPhO composite nanorods were rinsed in deionized water

* Corresponding author. Tel.: +60 1 92682768; fax: +60 3 79674146.
E-mail addresses: azzuliani@um.edu.my, azzuliani@yahoo.com (A. Supangat).

0167-577X/$ - see front matter © 2013 Elsevier B.V. All rights reserved.
http://dx.doi.org/10.1016/j.matlet.2013.12.058

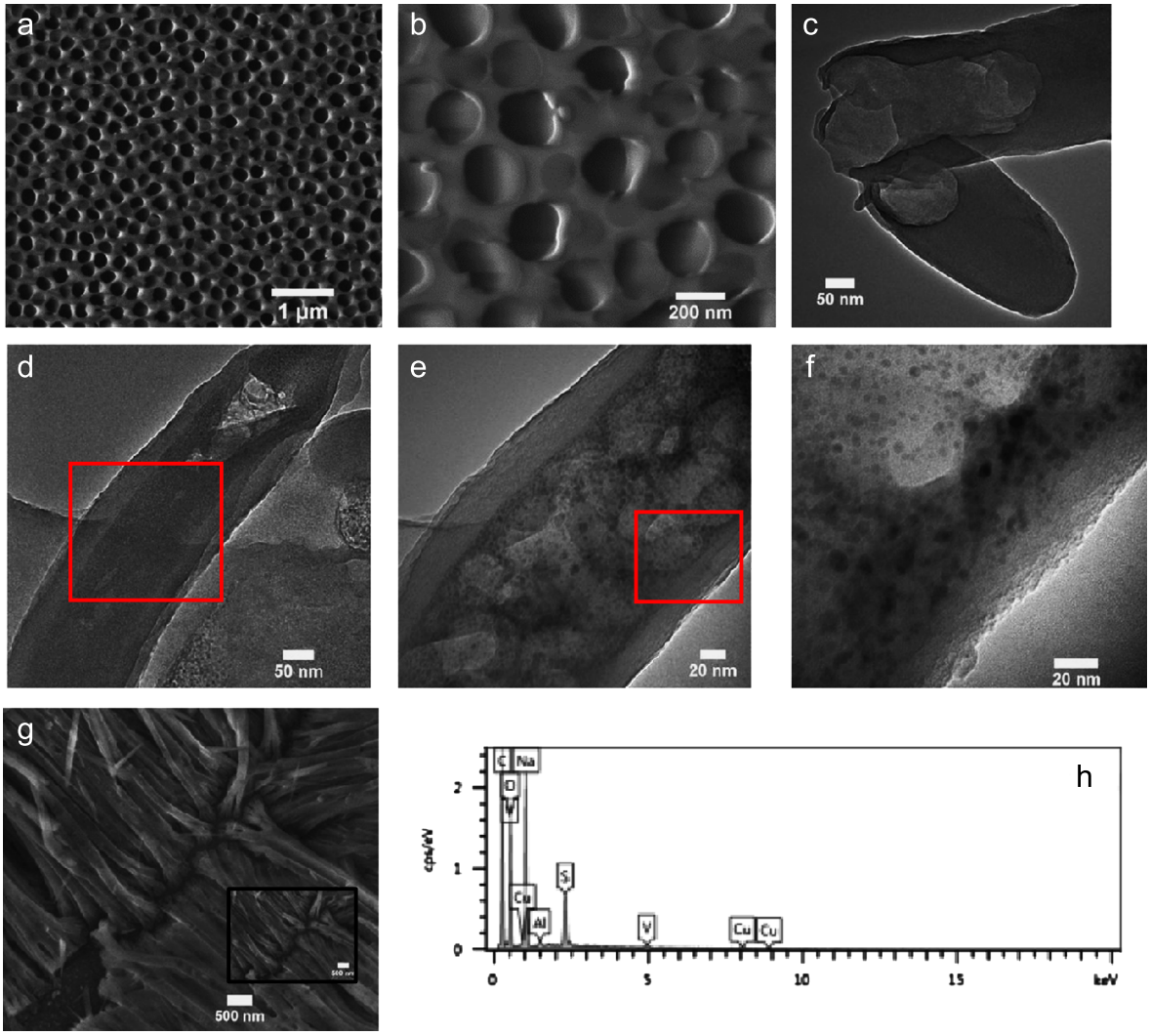

Fig. 1. (a) and (b) FESEM images of porous alumina template, (c) TEM image of P3HT nanotube, (d–f) TEM images of P3HT:VOPcPhO composite nanorods, (g) FESEM image of P3HT:VOPcPhO composite nanorods array (inset shows the high magnification image) and (h) EDX spectrum of P3HT:VOPcPhO composite nanorods.

prior to its characterisation. The P3HT:VOPcPhO composite nanorods were characterised by Field Emission Scanning Electron Microscopy (FESEM-EDX) (Quanta FEG 450), Transmission Electron Microscopy (TEM) (Tecnai G2 FEI), UV–vis spectroscopy (Shimadzu UV-3101PC), Raman and photoluminescence spectroscopy (RENISHAW).

3. Results and discussion

FESEM images of cleaned porous alumina template without any deposition of solution are shown in Fig. 1(a) and (b). The nominal template pore diameter is 200 nm and exhibits uniform rounded pores. Fig. 1(c) shows that P3HT nanotube has replicated the rounded structure of pores. The individual P3HT nanotube image that was captured from TEM has portrayed the identical diameter between the nanotubes and the template's pore size of about ~200 nm. The spin coating of P3HT solution onto the template has produced a coat at the inner diameter of the template without clogging through the pores. It seems that the low solution concentration of 5 mg/ml of P3HT could garner the low viscosity properties. This could allow VOPcPhO solution to infiltrate into P3HT nanotube and interfacial issue can be minimised.

A TEM image of an individual tubular VOPcPhO is shown in Fig. 1(d). Magnified view of the red box in Fig. 1(d) is illustrated in Fig. 1(e). TEM images of P3HT:VOPcPhO composite nanorod have shown a spectacular rod-shaped of regular wall with the representation of two different regions. The brighter region which acts as a shell corresponds to P3HT layer with thickness around ~20 nm. Whereby, the darker region corresponds to VOPcPhO and acts as a solid inner core of the composite nanorods structure. Significantly, this solid inner core of composite nanorod can be identified as VOPcPhO due to the appearance of visible domains of molecules aggregation and arrangement [12]. Fig. 1(f) presents the high-resolution TEM image of an individual tubular that has been magnified from the red box in Fig. 1(e). It suggests that there is an arrangement of VOPcPhO molecules within the composite nanorod. Visible domains revealed that VOPcPhO consists of regular spherical nanoparticles. The postulation on the formation of rod-shaped composite has been supported by the FESEM image that shown in Fig. 1(g). EDX spectrum of composite nanorods is shown in Fig. 1(h). Carbon (C), oxygen (O), sodium (Na), aluminium (Al), copper (Cu), vanadium (V) and sulphur (S) have been evidenced from the composite nanorods. EDX spectrum acquired from composite nanorods exhibits peaks of vanadium and sulphur which assigned to VOPcPhO and P3HT, respectively.

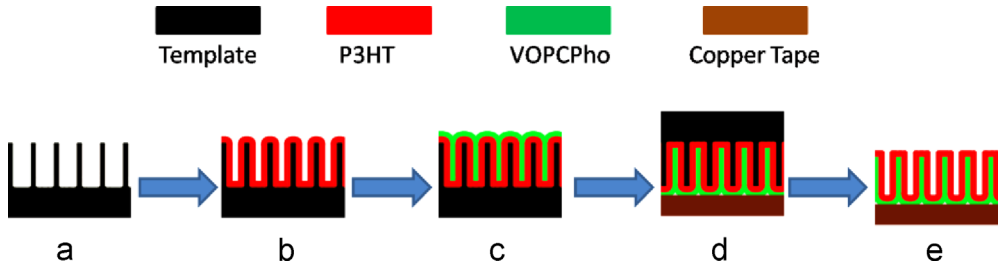

Fig. 2. Schematic illustration of the formation processes of P3HT:VOPcPhO composite nanorods.

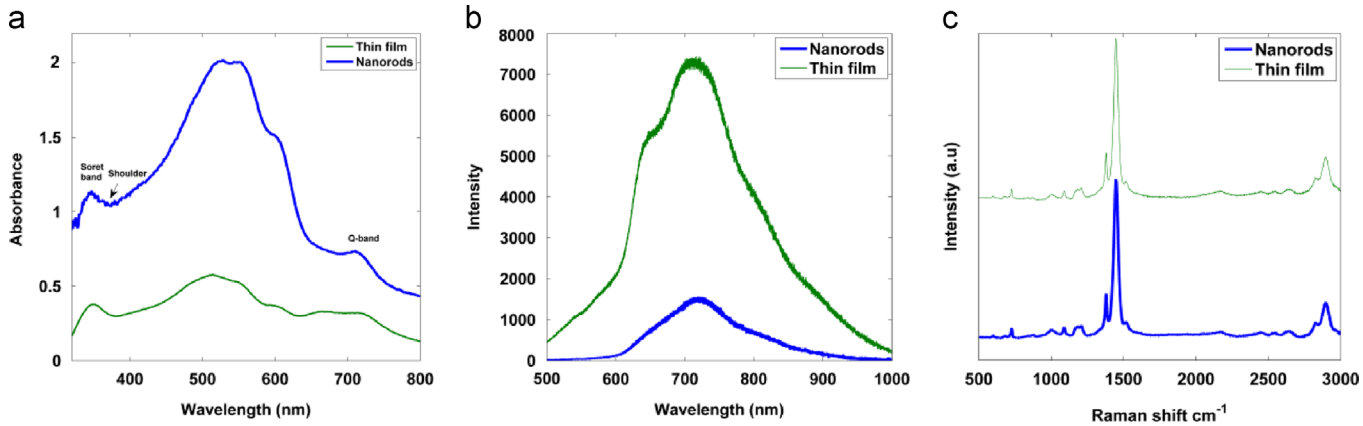

Fig. 3. (a) UV–vis absorption spectra (b) photoluminescence spectra and (c) Raman spectra of P3HT:VOPcPhO composite nanorods and thin films.

A schematic illustration of the proposed formation of P3HT:VOPcPhO composite nanorods is presented in Fig. 2. The alumina template was first cleaned to remove all the existing impurities that may block the template's pores (a). P3HT has been infiltrated into a template after the annealed process was applied at 150 °C (b). Then, the spin-coated of VOPcPhO taken place and infiltration can be observed (c). Before the dissolution of template, P3HT:VOPcPhO composite was attached to the copper tape which portrays the upside down formation (d). After the dissolution, P3HT:VOPcPhO composite nanorods were formed by replicating the template's channel (e).

Fig. 3(a) shows the UV–vis absorption spectra of P3HT:VOPcPhO composite nanorods and thin films. The intense absorption peaks at 528 nm and 553 nm with a shoulder at 591 nm is due to the existence of P3HT. The peak at 528 nm is due to the electron transition from the valence bond to the conduction band of P3HT. There is red shifted at the composite nanorods peak that due to P3HT which can be attributed to the increase of alkyl carbon chain in thiophene ring 3-substituted. Absorption bands that are due to VOPcPhO are assigned as Soret-band and Q-band which exist in the UV region between 347 and 376 nm and in the visible region between 643 and 752 nm, respectively [13]. The Soret-band exhibits similar peaks at 348 nm with a shoulder appear at 376 nm and 373 nm for both composite thin film and nanorod. A difference between P3HT:VOPcPhO composite nanorods and thin films spectrum has been observed at the Q-band of composite nanorods which a wider absorption range can be observed between 685 nm and 752 nm, as compared to composite thin films. The wider Q-band absorption (VOPcPhO) and red shift of peak absorption (P3HT) could be due to the presence of interaction between small molecules and conjugated polymer within the composite, well-distributed interface between two dissimilar nanostructured materials of small organic molecules of VOPcPhO and enhanced π–π* stacking of P3HT segment. In addition, the absorption pattern of Davydov splitting that occurred at Q-band has much influenced by the relative orientation of molecules [13]. At the Q-band of composite nanorods the stronger peak is occurred at 715 nm. This indicates that the first π–π* transition on the phthalocyanine macro-cycle is more dominant for the P3HT:VOPcPhO composite thin films rather than composite nanorods. Although the presence of first π–π* transition is observed by composite thin films, the improvement of second π–π* transition is exhibited by composite nanorods.

Photoluminescence spectra of P3HT:VOPcPhO composite nanorods and thin films are shown in Fig. 3(b). The photoluminescence intensity is totally quenched and red shifted in the composite nanorods. The distinguishable shift to the longer wavelength is occurred by 10 nm. Photo-induced charge transfer in composite nanorods is higher than composite thin films. It also indicates that the dissociation of charge carrier has occurred at the interface between P3HT:VOPcPhO composite nanorods. Raman spectra of P3HT:VOPcPhO composite nanorods and thin films are shown in Fig. 3(c). Similar absorption peaks at 2897 cm^{-1}, 1520 cm^{-1}, 1449 cm^{-1}, 1380 cm^{-1}, 1003 cm^{-1} and 727 cm^{-1} are observed which assigned for C–H stretching, C–C stretching, C=C stretching and C–H bending [14,15]. There are some minor shift in band wavenumbers between P3HT:VOPcPhO composite nanorods and thin film. The changes of band wavenumbers between composite nanorods and thin film are tabulated in Table 1. The Raman shift of C–H in-plane deformation vibration of composite nanorod is located at 1186 cm^{-1} and 1211 cm^{-1}, showing an apparent upward shift of about 4 cm^{-1} and 10 cm^{-1}, respectively.

4. Conclusions

In this work, P3HT:VOPcPhO composite nanorods have been synthesised by a simple solution process method via porous alumina template. Structural and optical properties of P3HT:VOPcPhO composite can be enhanced by means of nanorods structure.

Table 1
Raman peak positions of P3HT:VOPcPhO composite nanorods and thin films.

Raman shift (cm^{-1})		
Thin films	**Nanorods**	**Assignments**
727	727	Macrocycle stretching
1003	1003	Benzene ring breathing
1091	1088	C–H bending
1182	1186	C–H bending
1201	1211	C–H bending
1380	1380	C–C stretching
1449	1449	C═C stretching
1520	1520	Pyrole stretching
2897	2828	C–H stretching
2897	2897	C–H stretching

Acknowledgement

The authors would like to acknowledge University of Malaya and Ministry of Education Malaysia for the project funding under Fundamental research grant scheme (FP002-2013A) and University of Malaya High Impact Research Grant UM-MOHE (UM.C/625/3/HIR/MOHE/SCI/26).

References

[1] Ahmad Z, Abdullah SM, Sulaiman K. Measurement 2013;46:2073–6.
[2] Yang X, Wang Q, Zhang Y, Jiang Z. Polym J 2012;44:1042–7.
[3] Knizhnikova IS, Syromyatnikov VG, Vertsimakha YI, Verbitskii AB. Theor Exp Chem 2012;48:153–6.
[4] Touka N, Benelmadjat H, Boudine B, Halimi O, Sebais M. J Associ Arab Univ Basic Appl Sci 2013;13:52–6.
[5] Boland P, Sunkavalli SS, Chennuri S, Foe K, Abdel-Fattah T, Namkoong G. Thin Solid Films 2010;518:1728–31.
[6] Wang H-S, Lin L-H, Chen S-Y, Wang Y-L, Wei K-H. Nanotechnology 2009;20:1–5.
[7] Hatton RA, Blanchard NP, Stolojan V, Miller AJ, Silva SRP. Langmuir 2007;23:6424–30.
[8] Liu J, Wang Y, Sun DD. Mater Lett 2013;95:178–81.
[9] Cannon JP, Bearden SD, Gold SA. Compos: Part A 2010;41:836–41.
[10] Cheng S, Wei Y, Feng Q, Qiu K-Y, Pang J-B, Jansen SA, et al. Chem Mater 2003;15:1560–6.
[11] Hu J, Shirai Y, Han L, Wakayama Y. Nanoscale Res Lett 2012;7:469.
[12] Kamarundzaman A, Fakir MS, Supangat A, Sulaiman K, Zulfiqar H. Mater Lett 2013;111:13–6.
[13] Aziz F, Sayyad MH, Ahmad Z, Sulaiman K, Muhammad MR, Karimov KS. Physica E 2012;44:1815–9.
[14] Abdullah SM, Ahmad Z, Aziz F, Sulaiman K. Org Electron 2012;13:2532–7.
[15] Klimov E, Li W, Yang X, Hoffmann GG, Loos J. Macromolecules 2006;39:4493–6.